AD-A058 300 SRI INTERNATIONAL MENLO PARK CA F/G 13/13
CRITICAL LOADS FOR REINFORCED CONCRETE BUNKERS.(U)
NOV 77 A L FLORENCE DNA001-77-C-0181
UNCLASSIFIED DNA-4469F NL

1 OF 1
AD A058300

END
DATE FILMED
10-78
DDC

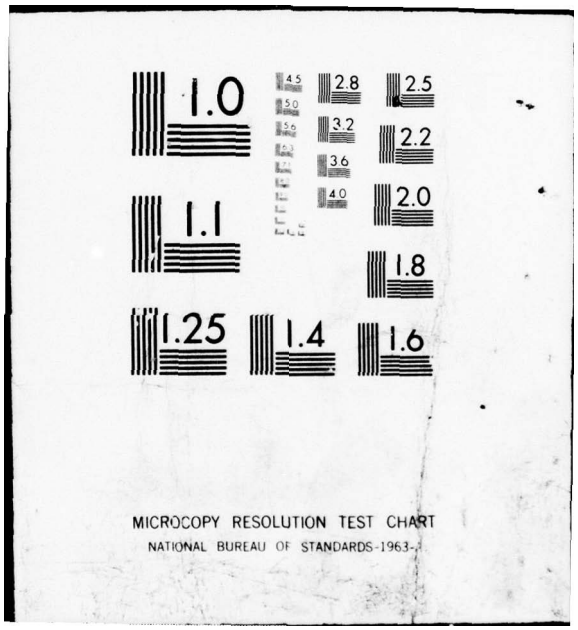
1.0
1.1
1.25
1.4
1.6
1.8
2.0
2.2
2.5
2.8
3.2
3.6
4.0
4.5
5.0
5.6
MICROCOPY RESOLUTION TEST CHART
NATIONAL BUREAU OF STANDARDS-1963-A

CRITICAL LOADS FOR REINFORCED CONCRETE BUNKERS

SRI International
333 Ravenswood Avenue
Menlo Park, California 94025

November 1977

Final Report for Period 7 March 1977—31 October 1977

CONTRACT No. DNA 001-77-C-0181

THIS WORK SPONSORED BY THE DEFENSE NUCLEAR AGENCY
UNDER RDT&E RMSS CODE B344077464 Y99QAXSC06222 H2590D.

Prepared for
Director
DEFENSE NUCLEAR AGENCY
Washington, D. C. 20305

Destroy this report when it is no longer needed. Do not return to sender.

(18) DNA, SBIE (19) 4469F, AD-E300 292

UNCLASSIFIED

SECURITY CLASSIFICATION OF THIS PAGE (When Data Entered)

REPORT DOCUMENTATION PAGE	READ INSTRUCTIONS BEFORE COMPLETING FORM
1. REPORT NUMBER: DNA 4469F ✓	2. GOVT ACCESSION NO. (9)
3. RECIPIENT'S CATALOG NUMBER	
4. TITLE (and Subtitle): (6) CRITICAL LOADS FOR REINFORCED CONCRETE BUNKERS	5. TYPE OF REPORT & PERIOD COVERED: Final Report, 7 Mar [redacted]—31 Oct 77
6. PERFORMING ORG. REPORT NUMBER: SRI PYU-6203	
7. AUTHOR(s): (10) A. L. Florence	8. CONTRACT OR GRANT NUMBER(s): (15) DNA 001-77-C-0181
(17) C062	
9. PERFORMING ORGANIZATION NAME AND ADDRESS: SRI International, 333 Ravenswood Avenue, Menlo Park, California 94025	10. PROGRAM ELEMENT, PROJECT, TASK AREA & WORK UNIT NUMBERS: (16) NWED Subtask Y99QAXSC062-22
11. CONTROLLING OFFICE NAME AND ADDRESS: (11) Director, Defense Nuclear Agency, Washington, D.C. 20305	12. REPORT DATE: Nov [redacted] 77
	13. NUMBER OF PAGES: 70
14. MONITORING AGENCY NAME & ADDRESS (if different from Controlling Office)	15. SECURITY CLASS. (of this report): UNCLASSIFIED (12) 71 p.
	15a. DECLASSIFICATION/DOWNGRADING SCHEDULE

16. DISTRIBUTION STATEMENT (of this Report)

Approved for public release; distribution unlimited.

17. DISTRIBUTION STATEMENT (of the abstract entered in Block 20, if different from Report)

18. SUPPLEMENTARY NOTES

This work sponsored by the Defense Nuclear Agency under RDT&E RMSS Code B344077464 Y99QAXSC06222 H2590D.

19. KEY WORDS (Continue on reverse side if necessary and identify by block number)

Nuclear	Shallow-Buried	Structures
Blast	Pressure Impulse	
Burst	Damage	
Bunker	Concrete	

20. ABSTRACT (Continue on reverse side if necessary and identify by block number)

Among the targets of interest for nuclear weapons are underground bunkers of reinforced concrete construction. The Defense Nuclear Agency is conducting a program to obtain the failure loads of shallow-buried bunkers subjected to air blast waves acting on the ground surface. The blast waves of interest are those from a nearby nuclear weapon of 1-kton yield detonated on or above the ground surface.

This report describes a simple conceptual framework for intrepreting experimental and theoretical load-damage results. This framework consists of

DD FORM 1 JAN 73 1473 EDITION OF 1 NOV 65 IS OBSOLETE

UNCLASSIFIED

SECURITY CLASSIFICATION OF THIS PAGE (When Data Entered)

20. ABSTRACT (Continued)

a Pressure-Impulse characterization of critical loads for the bunkers. The procedure for obtaining the characterization simplifies the prediction of damage to box bunkers caused by ground surface loading. It requires further development for improvement of the simplifying assumptions and comparisons of damage predictions with experimental results.

CONVERSION FACTORS FOR U.S. CUSTOMARY TO
METRIC (SI) UNITS OF MEASUREMENT

To Convert From	To	Multiply By
foot	meter (m)	3.084 x E-1
inch	meter (m)	2.540 x E-2
pound-force/inch^2(psi)	kilo pascal (kPa)	6.895

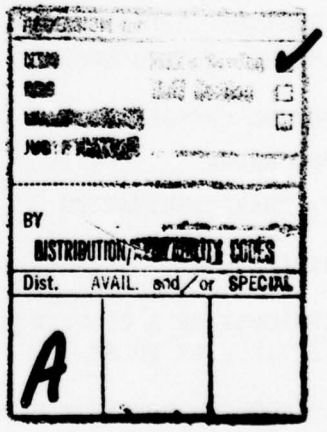

TABLE OF CONTENTS

ILLUSTRATIONS

1. INTRODUCTION AND SUMMARY

BACKGROUND

An experimental program is in progress at Waterways Experimental Station (WES) to determine failure loads of buried reinforced concrete box bunkers. In the WES experiments, the bunkers are 1/5- or 1/10-scale models, which have a soil cover of about half the bunker height. The main type of loading consists of high explosive simulation of ground surface blast loading from a nuclear weapon of 1-kton yield at 1/5- or 1/10-scale (Figure 1). The other type of loading consists of a spherical charge of TNT buried at bunker midheight and midlength (Figure 2).

The Defense Nuclear Agency (DNA) needs a simple conceptual framework for evaluating the experimental results and for providing a procedure for determining critical loads. The Pressure-Impulse (PI) characterization[1] is being investigated for this purpose. This report gives the status of this investigation.

OBJECTIVE

The objective of our work is to provide a PI characterization of critical loads for the box bunkers. The procedure for obtaining the PI characterization should allow prediction of the critical loads for other box bunkers.

REPORT ORGANIZATION

Section 2 describes PI characterization and outlines a simple procedure for approximating the effect of soil-structure interaction.

---

[1]G. R. Abrahamson and H. E. Lindberg, "Peak Load-Impulse Characterization of Critical Pulse Loads in Structural Dynamics," Nuclear Engineering and Design, 37 (1), 35-46 (1976).

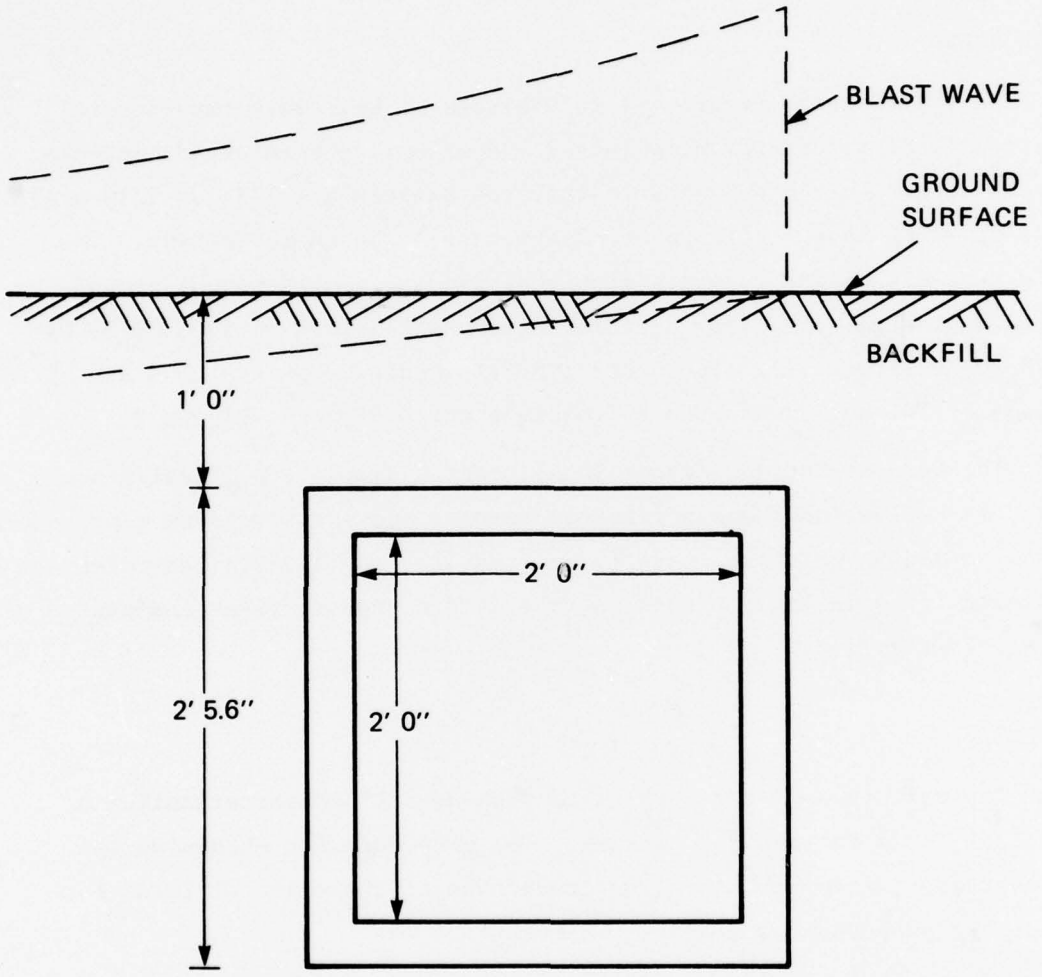

MA-6203-7

FIGURE 1 SURFACE LOADING TEST CONFIGURATION — DYNAMIC LOAD

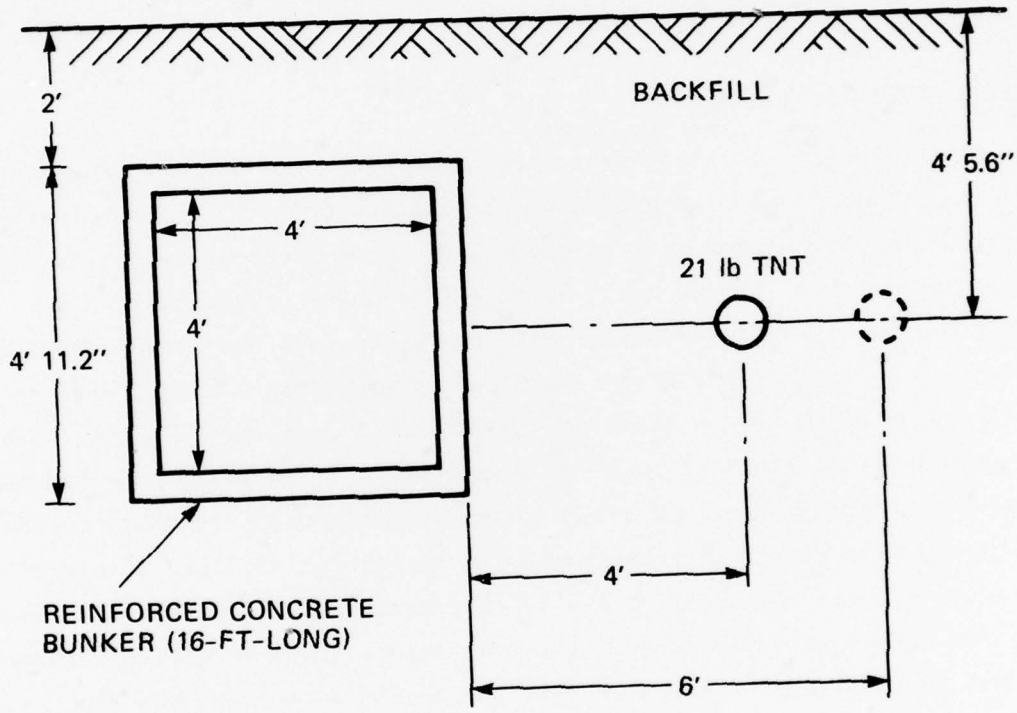

MA-6203-6

FIGURE 2 BURIED CHARGE TEST CONFIGURATIONS FOR 4-FOOT AND 6-FOOT RANGES

Section 3 develops the procedure for buried box bunkers subjected to ground surface blast loading. Section 4 contains the PI characterization of the buried box bunkers subjected to the loading from buried charges. Appendix A presents a dynamic rigid-plastic analysis of a clamped beam to provide a theoretical damage prediction and an approximate PI characterization. Appendix B is an outline of the derivation of the yield condition of the bunker slab; this yield condition is a relationship between the bending moment and thrust.

OVERALL RESULTS

A simple but very approximate method has been devised for providing a PI characterization of a buried box bunker subjected to a ground surface blast pulse. The approximations stem mainly from the representation of the soil-structure interaction. Because this phase of the WES experimental program is just beginning, only one static and one dynamic test have been performed; the dynamic test resulted in low damage. Thus, a PI characterization based on matching the universal structural PI curve* to the experimental results is not yet possible. The approximate method incorporates simple static and dynamic rigid-plastic analyses that provide damage predictions and approximations for the static collapse pressure and ideal impulse required for the PI characterization; the static collapse pressure agrees with the WES experimental result. The predicted permanent central deflection of the bunker roof in the WES experiment was high (1.2 inches compared with 0.5-inch central deflection on a 5.6 inch-thick, 4-foot-span bunker roof). This comparison provides an overall assessment of the assumptions that were used to simplify the method. Potential improvements are suggested below.

Figure 3 shows the PI characterization for ground surface blast pulses using the procedure developed in Section 3. The results given by the PI characterization and the WES dynamic experiment show that

*The universal PI curve is described in Section 2.

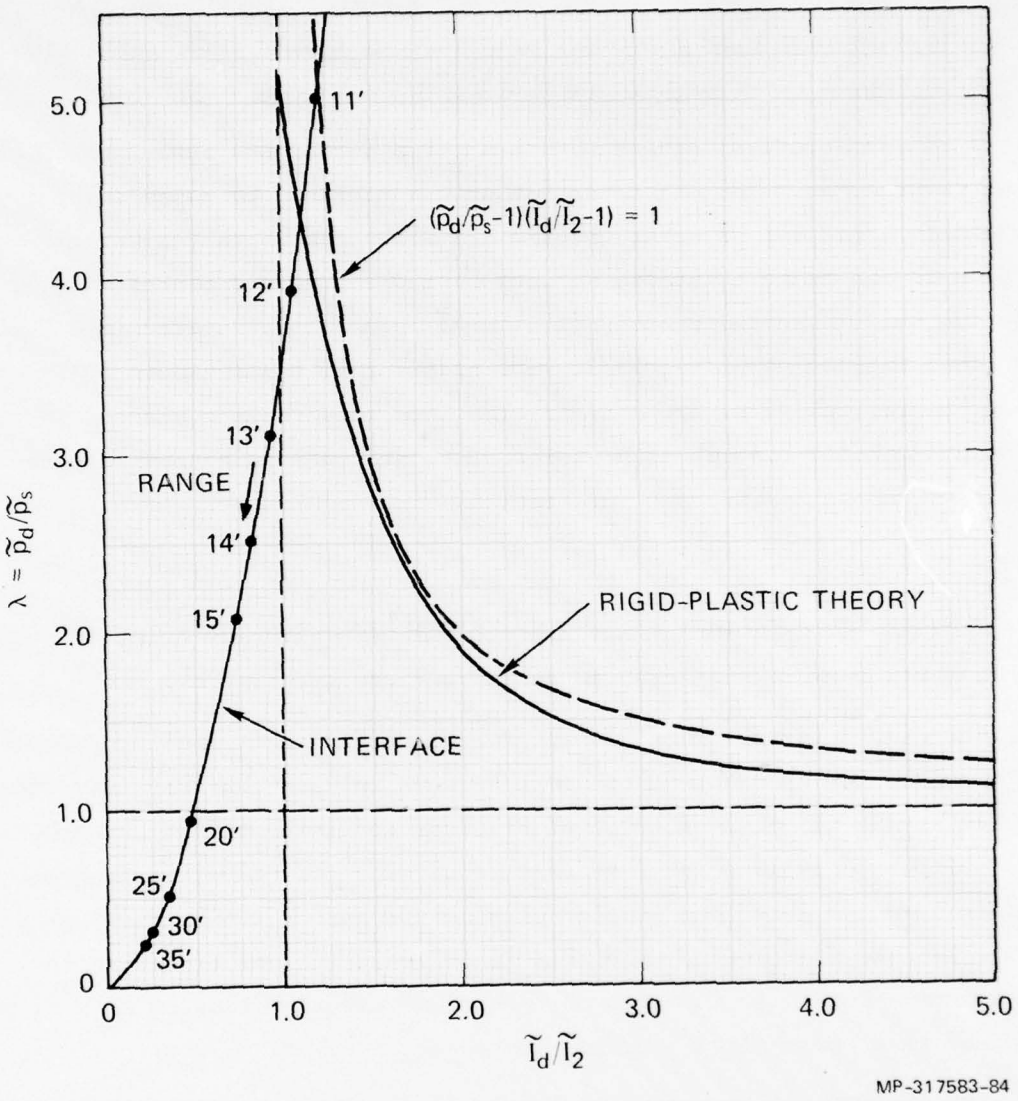

FIGURE 3 PI DIAGRAM FOR BUNKER AND SURFACE LOADING

the critical loads are highly impulsive and hence the range (distance between surface impact and the vertical middle plane of the bunker) is very short. Even for minor damage this range is less than six times the bunker roof or vertical dimension; for example, at 1/10-scale a 2 x 2 x 8 feet bunker is predicted to sustain a central roof deflection of 1 inch from a 1-ton nuclear surface burst at a range of 11 feet.

A PI characterization was obtained for a buried box bunker subjected to buried charges. The characterization was achieved by passing the universal structural PI curve through the interface PI values corresponding to the range (distance between buried charge and bunker face) for experimentally observed incipient failure; this matching determined I_o, the ideal impulse value required. The static collapse pressure P_o is the known theoretical value for a rigid-plastic clamped beam subjected to an assumed parabolic distribution of interface pressure to approximate the effect of the soil-structure interaction.

RECOMMENDATIONS

These recommendations concern the PI characterization of reinforced concrete box bunkers subjected to ground surface blast waves.

Whenever data become available from the WES dynamic loading experiments that allow at least an estimate of the incipient failure interface PI values, the universal structural PI curve should be passed through this point to determine the interface value of I_o as described in Section 2. To determine the interface static collapse pressure P_o, the existing results of the WES static loading experiment can be used. An an approximation, one can assume a parabolic interface pressure distribution that is zero at midspan and take the spatial averages to represent all PI values.

The theoretical treatment in Section 3 of this report should be continued to improve the assumptions, and an effort should be made to maintain the simplicity of the treatment. The assumptions that should be examined concern the following aspects:

- Blast pulse shapes
- Wave transit times
- Soil wave transmission and reflection
- Soil-structure interaction

A ground surface rectangular pulse is used in the procedure to simplify the analysis. The pressure and impulse are the same as the blast pulse, which is more closely represented by an exponential decay following the instantaneous rise to peak pressure. At the important impulsive end of the PI curve, the pulse shape is not important; hence, the existing analysis should be extended with a rectangular pulse to treat pressures higher than 5.3 times the static collapse pressure.

Another analytical simplification in the procedure is the assumption that the roof thrust from the lateral pressure on the bunker is applied only while the vertical interface pressure is acting. For highly impulsive, short-duration loads, this assumption is weak because of the time taken for the pulse to pass from the top to the bottom of the bunker; thus, the analysis should be modified to account for the wave transit time. This step will introduce the soil bulk modulus and density into the procedure.

Currently we have not taken into account either the attenuation of the pulse as it propagates downward through the soil or the pulse shape change or reflection from the bunker roof; these features should be modeled in a simplified manner for inclusion in the procedure.

Inclusion of soil-structure interaction is currently modeled as a simple redistribution of pressure from a uniform incident pulse to a parabolic interface pulse. This assumption should be examined for improvement. For example, the WES experiments suggest that a uniformly distributed impulse followed by a parabolically distributed pressure pulse may be more realistic.

We recommend strongly that a pilot experimental program be initiated, using bunker models at about 1/40-scale, to run in parallel with the WES

experimental program. Models of reinforced concrete bunkers at this scale are practical and the experimental program would generate data economically and rapidly, provide validation for the PI characterization, and allow assessment of the influence of various geometric and mechanical parameters; other bunker shapes can be fabricated and tested (arches, for example). The observations would be useful in the planning of tests at larger scales.

2. PRESSURE-IMPULSE CHARACTERIZATION OF BUNKERS

CONCEPT

Figure 4 shows schematically the construction procedure for a pressure-impulse (PI) diagram. Figures 4a and 4b show the variations of ground surface peak pressure and impulse with range from a specified nuclear weapon; Brode[2,3] provides relationships giving these variations. Figure 4c shows the "free-field" or surface PI relationship that results when the range is eliminated from the plotting coordinates; range becomes an intrinsic coordinate that is measured along the curve and increases as the PI origin is approached. For buried structures, the PI loading is the interface pressure and impulse. Thus, to obtain the interface PI curve shown in Figure 4c from the free-field or surface PI curve, a procedure is required that is based on the mechanics of load transfer and includes soil-structure interaction. Again, range is an intrinsic coordinate.

The curve labeled "structure" in Figure 4c is an isodamage curve for a specified structure in that it contains all combinations of peak pressure and impulse for a specified pulse shape that produce the same level of damage. From experiments and analyses of simple structures subjected to pulse loading, we have shown[1] that the structural PI curve has the general form shown in Figure 4c.

The interface and structural PI curves intersect at a point having a range value that is the intrinsic coordinate on the interface PI curve.

---

[2]H. L. Brode, "Review of Nuclear Weapons Effects," Annual Review of Nuclear Science, 18, 153-202 (1968).

[3]H. L. Brode, "Height of Burst Effects at High Overpressures," DASA Report 2056, July 1970.

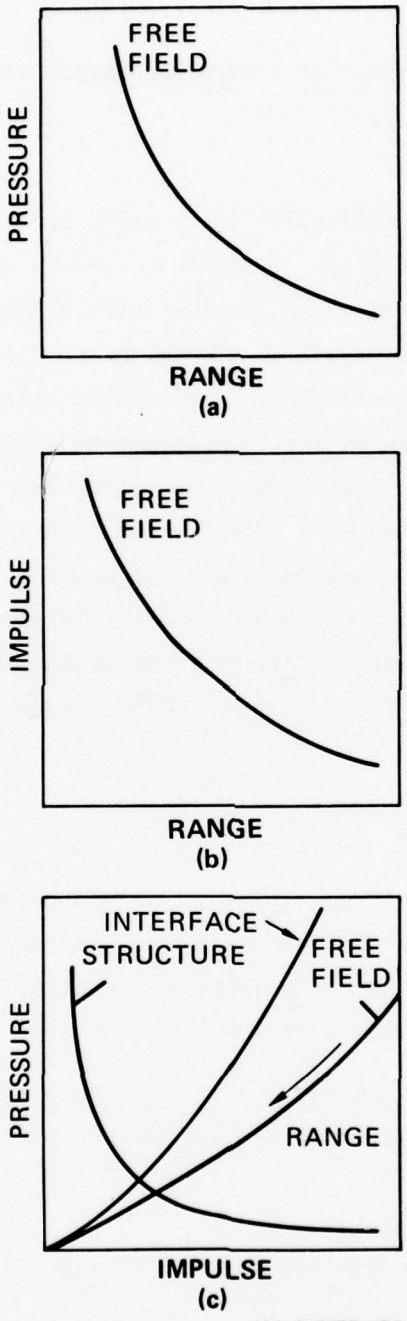

FIGURE 4 PI PREDICTIVE METHOD FOR BURIED STRUCTURE FAILURE

If the isodamage curve is the PI curve for failure of the structure, the point of intersection gives the range within which the specified nuclear weapon will destroy the structure.

Past work on PI characterization[1] has included an approximate generalization of the structural PI curve. The pressure and impulse are usually plotted in terms of the ratios P/P_o and I/I_o, where P_o is the static collapse pressure and I_o is the ideal impulse to produce the same damage as that associated with the isodamage curve. An approximation of the curves of many simple structures is

$$(P/P_o - 1)\ (I/I_o - 1) = 1 \tag{1}$$

Thus, an approximate PI curve is established if P_o and I_o are determined by special tests or approximate analysis. If, during a test series, values of P_1 and I_1 are measured that produce incipient structural failure, only one of the two quantities P_o and I_o must be determined. If a special static test is used to determine P_o, Eq. (1) gives for I_o,

$$I_o = I_1 \frac{P_1/P_o - 1}{P_1/P_o} \tag{2}$$

INTERFACE PI CURVE

For a specified bunker, soil, and burial depth, a series of experiments in which the surface PI curve is used could provide the PI characterization. The experiments would have to include the surface pressure P_o required to cause static failure of the bunker and a pair of values P_1, I_1 for the surface pulse that causes dynamic failure of the bunker; the value of I_o could then be calculated by (2). However, this procedure assumes that the structural PI curve given by (1) applies to buried structures and it provides neither a method of generalizing the result to other bunker designs nor an understanding of the mechanisms involved.

Thus, a procedure is required to generate an interface PI curve that accounts for the mechanisms of load transfer from the surface to the bunker.

The load transfer process consists of transmission of the surface pulse downward through the soil, reflection and diffraction from the bunker, and the resulting soil-structure interaction. This complex process transforms the fairly uniform surface pulse into an interaction pulse having a different peak pressure, shape, and distribution. If a general procedure is to be formulated for determining the interface PI curve from the free-field PI curve, we must introduce simplifying assumptions to reduce the complexity of the load transfer mechanics. These assumptions must lead to results that agree approximately with experimental results. Also, the procedure requires a choice of definition of the interface pressures and impulses because of the spatial variations. The development and application of the procedure is the subject of Section 3.

3. SURFACE BLAST LOADING

We develop here the procedure to obtain a Pressure-Impulse (PI) characterization of a shallow-buried box bunker subjected to surface blast loading. The procedure is summarized at the end of this section. Calculations are based on the design shown in Figure 5 which, for the purpose of illustrating the procedure, is assumed to be 1/10 scale. Calculations are also based on a 1 kton surface burst reduced to 1/10 scale to correspond to the assumed scale of the box bunker design.

GROUND SURFACE PRESSURE PULSE

Approximate formulas[2] relating the peak pressure, impulse, range, and yield (P, I, R, W) are given in psi, psi-sec, kft, and Mton units, respectively, are

$$P = 3300\ W/R^3 + 192\ W^{1/2}/R^{3/2} \tag{3}$$

$$I = 1.83\ P^{1/2}\ W^{1/3}\ [1 + 0.00385P^{1/2}] \tag{4}$$

Figures 6, 7, and 8 show the pressure-range, impulse-range, and pressure-impulse curves that result from formulas (3) and (4) for a surface burst of 1-ton yield, which is the 1/10-scale yield for a 1-KT full-scale yield. The results in Figures 6, 7, and 8 are in approximate agreement with the corresponding results from reference 3. A plot of the pulse duration[3] (period of positive overpressure) is shown in Figure 9. An example of the pulse shape[3] is shown in Figure 10.

Analysis of the dynamic response of rigid-plastic structures to blast loading can be greatly simplified by replacing the blast pulse by a rectangular pulse with the same peak pressure and impulse; by this method, however, damage is overpredicted for pulses with durations comparable to the fundamental structural period; for rigid-plastic structures, this fundamental structural period may be taken as the duration of motion. However, calculations presented below indicate that durations of pulses causing failure are much shorter than durations of motion and are therefore impulsive.

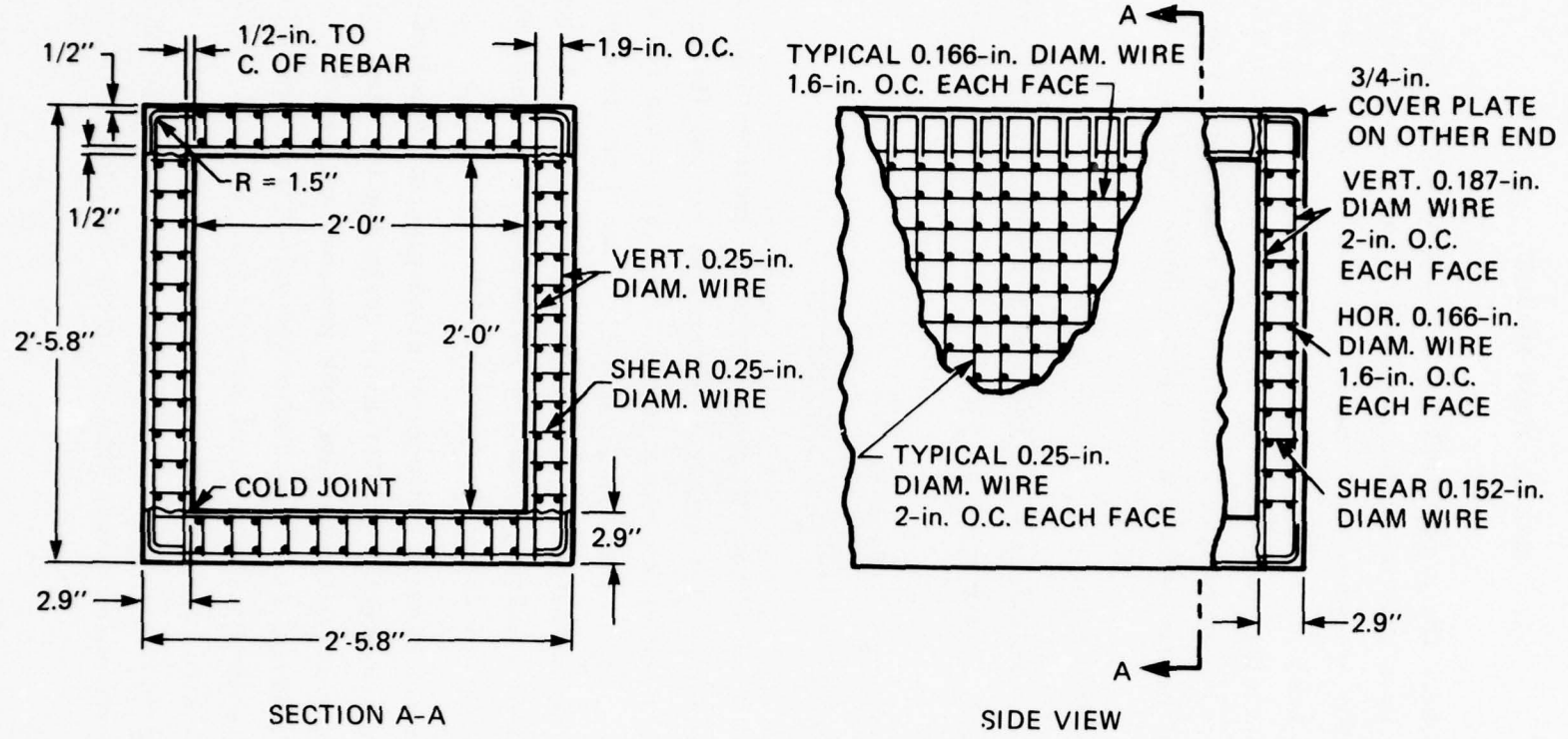

MA-6203-9

FIGURE 5 RECTANGULAR BOX STRUCTURE (L/D = 10)

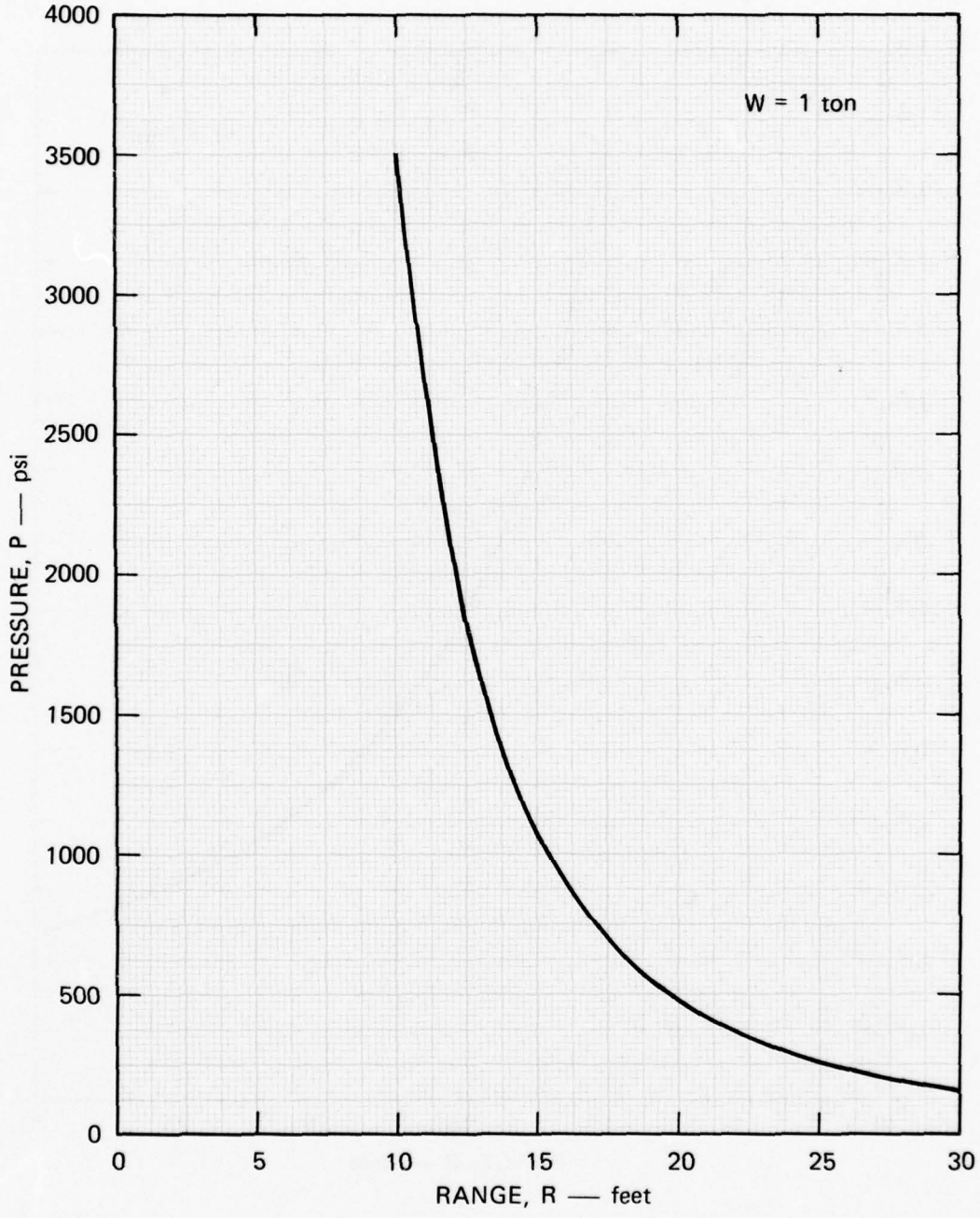

FIGURE 6 PRESSURE-RANGE RELATIONSHIP

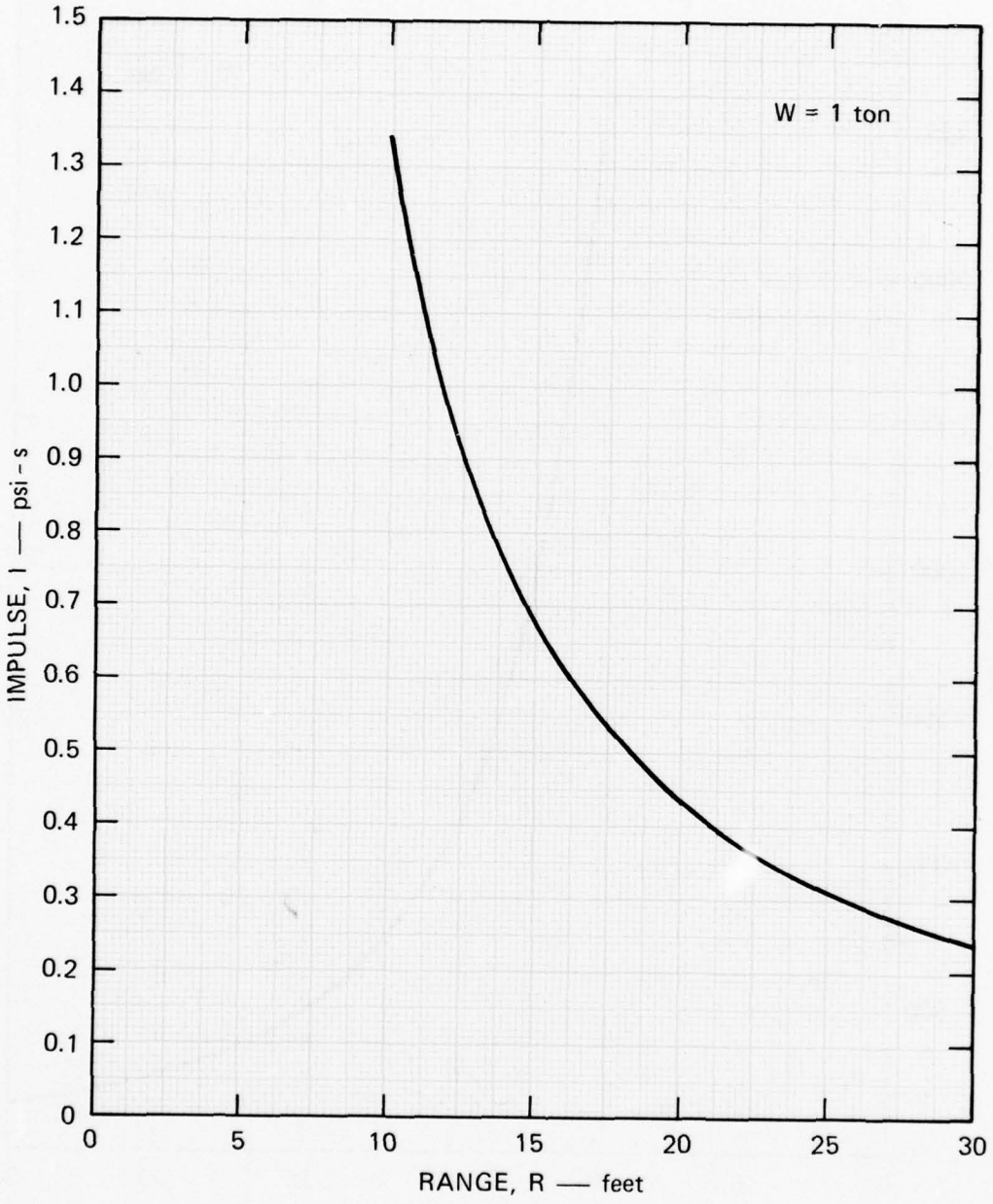

MA-6203-11

FIGURE 7 IMPULSE-RANGE RELATIONSHIP

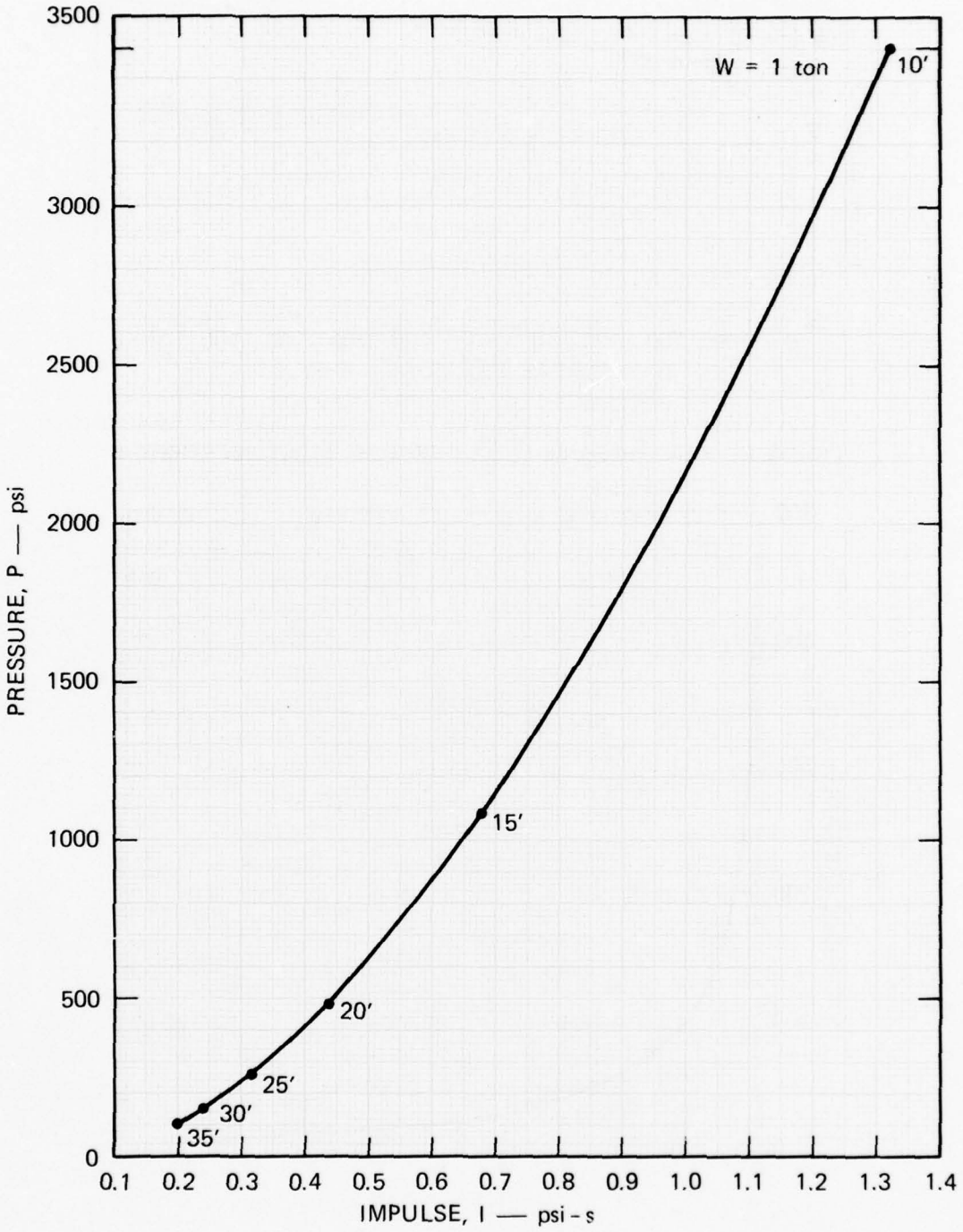

MA-6203-12

FIGURE 8 PRESSURE-IMPULSE RELATIONSHIP

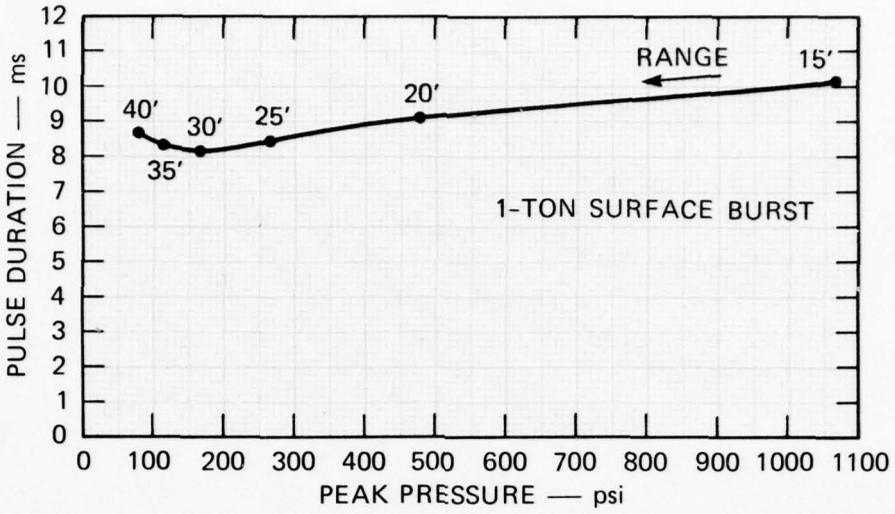

MA-6203-13

FIGURE 9 PEAK PRESSURE-PULSE DURATION-RANGE RELATIONSHIP

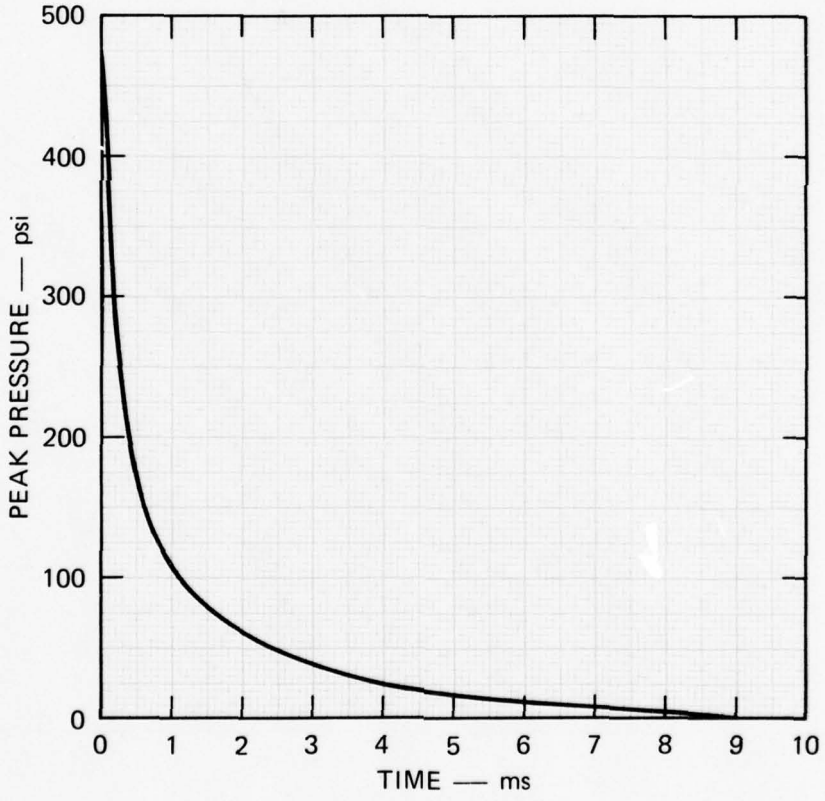

MA-6203-14

FIGURE 10 PRESSURE PULSE 20 FEET FROM 1-TON SURFACE BURST

INTERACTION PRESSURE AND IMPULSE

As trial approximations, the effects of the soil-structure interactions are taken as: (1) a redistribution of pressure from a uniform distribution on the ground surface to a parabolic distribution on the bunker roof, having the minimum pressure at the center and the maxima at the edges, and (2) a preservation of the pulse duration and pulse shape. The average pressure of the parabolic pressure distribution is equated with surface pressure, as is the pulse duration. The influence of the blast wave transit time is neglected.

From the infinite possibilities of parabolic distributions of pressure, we have chosen the one producing no interaction pressure at the roof center because it maximizes the load required to cause a specified damage.

For the box design shown in Figure 5, which has internal dimensions of 24 x 24 inches and a wall thickness h = 2.8 inches, the parabolic pressure distribution is

$$P = q_2\left(\frac{x}{\ell}\right)^2 \tag{5}$$

where ℓ = 12 inches is regarded as the half-span of a clamped beam modeling the roof. The average pressure on the entire top surface of length $2\ell + 2h$ is

$$P = \frac{1}{\ell+h}\int_0^{\ell+h} p(x)dx = \frac{1}{3}\,q_2\left(\frac{\ell+h}{\ell}\right)^2$$

and, by assumption, equals the corresponding uniform ground surface pressure. The average pressure on the clamped beam of length 2ℓ is

$$\tilde{P}_d = \frac{1}{\ell}\int_0^{\ell} p(x)dx = \frac{1}{3}\,q_2 \tag{6}$$

Hence, the interaction pressure required in the PI characterization is

$$\tilde{P}_d = \left(\frac{\ell}{\ell+h}\right)^2 P \tag{7}$$

which, for the bunker of Figure 5, gives

$$\tilde{P}_d = \frac{2}{3} P \tag{8}$$

Preservation of the pulse shape and duration gives

$$\tilde{I}_d = \frac{2}{3} I \tag{9}$$

As a numerical example, Table 1 gives the surface pressure and impulse at a range of 20 feet as P = 479 psi, and I = 0.414 psi-s so that, by Eqs. (8) and (9), the interaction pressure and impulse are $\tilde{P}_d$ = 319 psi and $\tilde{I}_d$ = 0.276 psi-s. The pressure over the clamped beam supports at $x = \pm\ell$ is $q_2 = 3p_d$ = 957 psi; over the edge of the bunker at $x = \pm\ell\ (\ell + h)$, the pressure is 1456 psi.

TABLE 1 PULSE DATA FOR 1-TON SURFACE BURST

Range (ft)	Peak Pressure (psi)	Impulse (psi-s)	Pulse Duration (ms)	Equivalent Rectangular Pulse Duration (ms)
15	1064	0.623	10.11	0.586
20	479	0.414	9.11	0.864
25	266	0.297	8.45	1.117
30	168	0.226	8.21	1.345
35	114	0.182	8.32	1.597
40	83	0.153	8.71	1.843

THRUST ON ROOF SLAB

In the soil away from the side of the bunker, the horizontal and vertical compressive stresses σ_x and σ_y become the principal stresses. If these stresses cause distortional yielding of the soil according to the Mohr-Coulomb criterion, they satisfy the relationship

$$\sigma_x = \frac{1 - \sin\phi}{1 + \sin\phi}\sigma_y - \frac{2c\cos\phi}{1 + \sin\phi} \tag{10}$$

where ϕ and c are the friction angle and cohesive strength of the soil, respectively. Away from the bunker side, we assume that the place wave descending into the soil is replaced by a pressure pulse acting instantaneously along the full height of the bunker so that $\sigma_y = P(t)$, the surface pressure pulse. The other stress component σ_x is given by Eq. (10). This uniformly distributed lateral pressure is redistributed on the side of the bunker because of the structural response, but the average pressure is taken to be σ_x and is assumed to act as long as the roof is being loaded from above. The thrust produced by this quasi-static model is therefore $N = (\ell + h)\sigma_x$. The consequences of neglecting wave propagation are not considered in this analysis.

For soil with $\phi = 35°$ and c = 10.7 psi, Eq. (10) becomes

$$\sigma_x = 0.271\sigma_y - 11 \tag{11}$$

For a surface pressure of $\sigma_y = P = 479$ psi, we have $\sigma_x = 119$ psi; hence, the bunker of Figure 5 (ℓ = 12 in., h = 2.8 in.) receives a roof thrust of N = 1758 pounds.

MOMENT-THRUST YIELD CONDITION

In the analysis of Appendix B, Figure B3 shows the moment-thrust yield condition for the bunker roof slab. The data used are as follows:

Slab depth	h = 2.8 in.
Reinforcement spacing	b = 2.0 in.
Upper steel depth	d^1 = 0.4 in.

Lower steel depth	$d = 2.4$ in.
Diameter of steel bars	$d_s = 0.25$ in.
Area of steel bars	$A_s = \pi d_s^2/4 = 0.049$ in.^{2}
Steel modulus	$E_s = 28 \times 10^6$ lb/in.^{2}
Concrete modulus	$E_c = 3.5 \times 10^6$ lb/in.^{2}
Modular ratio	$n = E_s/E_c = 8$
Steel yield strength	$\sigma_y = 72{,}000$ psi
Concrete crush strength	$\sigma_u = 6{,}000$ psi
Strength ratio	$S = \sigma_y/\sigma_u = 12$
Steel area ratio	$\alpha = A_s/bh = 0.00877$

The fully plastic moment and thrust per unit slab width were found to be

$$M_o = 4102 \text{ lb.in./in.} \qquad N_o = 20{,}042 \text{ lb./in.}$$

An approximation to that portion of the yield condition for $0 < N/N_o < 0.1$ is

$$\frac{M}{M_o} = 1 + 5\frac{N}{N_o} \qquad 0 < \frac{N}{N_o} < 0.1 \tag{12}$$

STATIC COLLAPSE

The parabolic pressure distribution (see Eq. 5) applied statically to a clamped rigid-plastic beam causes collapse in a three-hinge mechanism when the average pressure becomes

$$\tilde{P}_s = \frac{8M}{\ell^2} \tag{13}$$

If we neglect thrust initially and use the fully plastic moment M_o in Eq. (13), the static collapse pressure is $P_s = 228$ psi. Equation (7) relates the average interaction pressure to the surface pressure P, so that

$$P = \left(\frac{\ell+h}{\ell}\right) P_s = \frac{3}{2} P_s = 342 \text{ psi}$$

as a first approximation.

Inserting this value for σ_y in Eq. (11) gives the average pressure on the side of the bunker as σ_x = 83 psi, resulting in a thrust on the roof slab of N = 1,228 lb./in. By Eq. (12), this thrust (N/N_o = 0.061) increases the resistive moment to M = 1.31 M_o, the average interaction pressure to $\tilde{P}_s$ = 298 psi, and the surface pressure to P = 446 psi, as a second approximation. Three further iterations give N/N_o = 0.10, M/M_o = 1.51, $\tilde{P}_s$ = 344 psi, and P = 516 psi. This surface pressure compares reasonably well with the results of the WES static test conducted with the configuration of Figure 11.

DYNAMIC COLLAPSE

Appendix A presents an analysis of the response of a clamped rigid-plastic beam to a rectangular pulse with a parabolic distribution symmetric about the center; the pressure is zero at the beam center. The results provide a theoretical prediction of the central deflection and duration of motion for comparison with the results of the WES dynamic experiment. The analysis also provides guidance for the selection of an impulse to play the role of I_o in a PI characterization; the analysis is not complete, but it treats pressures up to five times the static collapse pressure.

The final central deflection and motion duration formulas obtained are

$$W_f = \frac{\tilde{p}_d t_d^2}{2\mu} \bar{\rho}_1^2 \left[1 + \frac{4}{3} \lambda m_s \bar{\rho}_1^2 \left\{2 - \left(1 - \rho_1\right)^2\right\}\right] \tag{14}$$

$$\frac{t_f}{t_d} = 1 + \frac{2}{3} \lambda m_s \bar{\rho}_1^2 \left\{3 - \left(1 - \rho_1\right)^2\right\} \tag{15}$$

where

$$\left(1 - \bar{\rho}_1\right)^2 \left(3 + 6\bar{\rho}_1 + 5\bar{\rho}_1^2\right) = \frac{3m_d}{m_s} \tag{16}$$

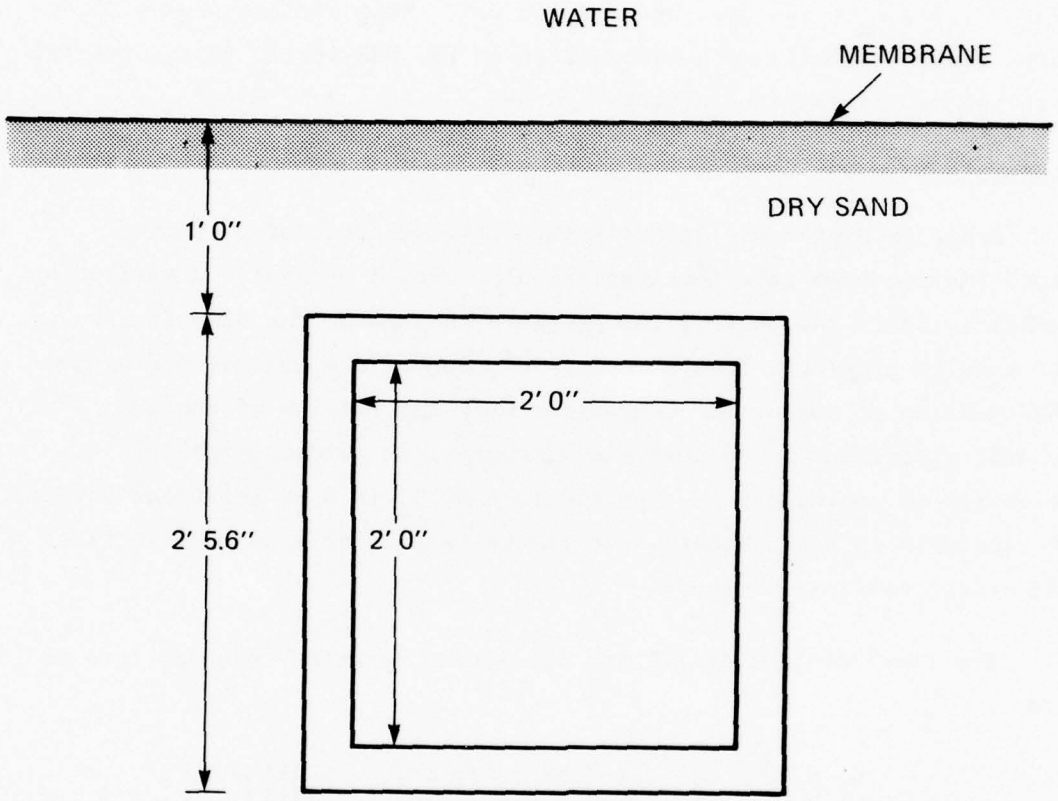

MA-6203-8

FIGURE 11 SURFACE LOADING TEST CONFIGURATION — STATIC LOAD

The range of λ is $1 < \lambda < 5.3$ for the structure of Figure 5. The symbols denote

W_f: central deflection

p_d: average pressure on beam

t_d: rectangular pulse duration

μ: beam mass per unit length

$\bar{\rho}_1$: dimensionless initial location of plastic hinge ($\bar{\rho}_1 = \bar{x}_1/\ell$, where ℓ is the half-span)

λ: pressure ratio ($\lambda = \tilde{p}_d/\tilde{p}_s$, where $\tilde{p}_s$ is the static collapse pressure)

m_s: static moment ratio ($m_s = M_s/M_o$, where M_s and M_o are the yield moments at static collapse with and without thrust)

m_d: dynamic moment ratio ($m_d = M_d/M_o$, where M_d and M_o are the yield moments during dynamic collapse with and without thrust).

t_f = beam motion duration.

COMPARISON WITH WES EXPERIMENT

The WES dynamic test, Essex Box HEST 1 (9 August 1977) was performed on a reinforced concrete box having the internal dimensions of 4 x 4 x 16 feet. For our comparison, the WES data are scaled to apply to a bunker with internal dimensions of 2 x 2 x 8 feet. The box design is now given by that shown in Figure 5, which we again assume to be 1/10 scale.

The deflection predicted is obtained as follows:

- Measured peak surface pressure (WES gage BP3), P = 1800 psi
- Measured surface impulse, $I = \frac{1}{2} \times 3.6 = 1.8$ psi-s
- Duration of equivalent rectangular pulse, $t_d = I/P = 1$ ms
- From Eqs. (8) and (9), the average interface pressure and impulse are

  $\tilde{p}_d = 1200$ psi $\tilde{I}_d = 1.2$ psi-s
- Average interface static collapse pressure, $p_s = 344$ psi (This pressure corresponds to a static surface pressure of P = 516 psi)
- Pressure ratio $\lambda = \tilde{p}_d/\tilde{p}_s = 3.49$, so $1 < \lambda < 5.3$.

- Initial location of plastic hinges, from (16), is $\bar{\rho}_1 = 0.61$
- Central deflection, from (14), is $W_f = 2.06$ in.
- Duration of motion, from (15), is $t_f = 4.72$ ms.

As a reasonable single correction when the impulse applied during motion is less than the total impulse, let the impulse be that at $t_f = 4.72$ ms; that is, I = 1.5 psi-s. Then

$$W_f = 1.44 \text{ in.} \qquad t_f = 3.95 \text{ ms}$$

For the WES bunker the predicted deflection is 2.85 inches, whereas the experimental deflection is 0.5 inch; thus, the prediction is too high. The method therefore has to be examined to account for the high deflection prediction. The approximation that definitely leads to high deflections is the replacement of the blast pulse by a rectangular pulse with the same peak pressure and impulse.

A less approximate method of choosing the rectangular pulse is first to consider the experimental pulse shape as an initial spike supposed on an exponential pulse. The impulse associated with the pressure spike is only about 5% of the total impulse. Hence, we consider the whole pulse as an exponential pulse with the same total impulse. We determine the peak pressure and decay parameters P_o and α by matching the experimental impulses at two different time points. This new peak pressure is used for the rectangular pulse; the impulse is still the same. Mathematically, the pulse may be expressed as

$$P = P_o e^{-\alpha t}$$

so the corresponding impulse is

$$I = I_\infty (1 - e^{-\alpha t})$$

where

$$I_\infty = P_o/\alpha$$

and is the total impulse. For I_∞ = 1.8 psi-s and I = 1.0 psi-s at time t = 2 ms, we have $\alpha = 102\ s^{-1}$ and P_o = 730 psi. The above deflection prediction procedure then gives

t_d = 2.46 ms, $\tilde{p}_d$ = 487 psi, λ = 1.41, $\bar{\rho}_1$ = 0.36

t_f = 3.66 ms

W_f = 0.97 in.

As a single correction, when the impulse applied during motion is less than the total impulse, let the impulse be that at t_f = 3.66 ms; that is, I = 1.4 psi-s. Then the central deflection and motion duration are

W_f = 0.58 in. $\qquad$ t_f = 2.83 ms

The above procedure for a more reasonable choice of the rectangular pulse results in a predicted deflection of 1.16 inches for the WES bunker, which is much closer to the experimental value of 0.5 inch than the previous prediction of 2.85 inches.

PRESSURE-IMPULSE CHARACTERIZATION

The analysis of Appendix A treats the structural response of a clamped rigid-plastic beam to a rectangular pressure pulse with a symmetric parabolic distribution about the center; the pressure is zero at the center. The interaction pressure is the spatial average of the distributed peak pressures. For the 1/10-scale bunker of Figure 5, the static interaction pressure is $\tilde{p}_s$ = 344 psi. The analysis is applicable up to a pressure parameter value of λ_2 = 5.27, which corresponds to an interaction pressure of $\tilde{p}_d$ = 1810 psi. According to the assumption of the roof peak load being the same aa the ground surface load, the analysis is applicable up to a ground surface pressure of P = 2715 psi; the corresponding range and impulse are 11 feet and 1.1 psi-s at 1/10-scale (Figures 6 and 7). The duration of the equivalent rectangular pulse is 0.4 msec, so that the loading is highly impulsive when $\lambda = \lambda_2$.

We rewrite the deflection formula (14) as

$$W = \frac{\tilde{I}^2}{2\mu\tilde{p}_s} \cdot \frac{\bar{\rho}^2}{\lambda} \cdot \left[1 + \frac{4}{3}\lambda m_s \bar{\rho}^2\{2 - (1 - \bar{\rho})^2\}\right] \tag{17}$$

where $I = p_d t_d$ and $\bar{\rho}$ is written instead of $\bar{\rho}_1$. When $\lambda = \lambda_2$, formula (17) may be written as

$$W_2 = \frac{\tilde{I}_2}{2\mu\tilde{p}_s} \cdot \frac{\bar{\rho}_2^2}{\lambda_2} \cdot \left[1 + \frac{4}{3}\lambda_2 m_s \bar{\rho}_2^2\{2 - (1 - \bar{\rho}_2)^2\}\right] \tag{18}$$

where $\bar{\rho}_2$ is the location of the plastic hinge when $\lambda = \lambda_2$. We choose W_2 as the central deflection required for structural failure to determine I_2, which now plays the role of the ideal impulse I_o in the PI characterization. The isodamage or structural PI curve is obtained by letting $W = W_2$. Thus, equating formulas (17) and (18) gives

$$\left(\frac{\tilde{I}}{\tilde{I}_2}\right)^2 = \frac{\lambda\bar{\rho}_2^2\left[1 + \frac{4}{3}\lambda_2 m_s \bar{\rho}_2^2\{2 - (1 - \bar{\rho}_2)^2\}\right]}{\lambda_2\bar{\rho}^2\left[1 + \frac{4}{3}\lambda m_s \bar{\rho}^2\{2 - (1 - \bar{\rho})^2\}\right]} \tag{19}$$

where $\bar{\rho}$ is a function of λ.

Figure 12 shows the structural curve of formula (19) along with the universal structural PI curve of formula (1) where $\tilde{I}_2$ takes the part of the ideal impulse I_o.

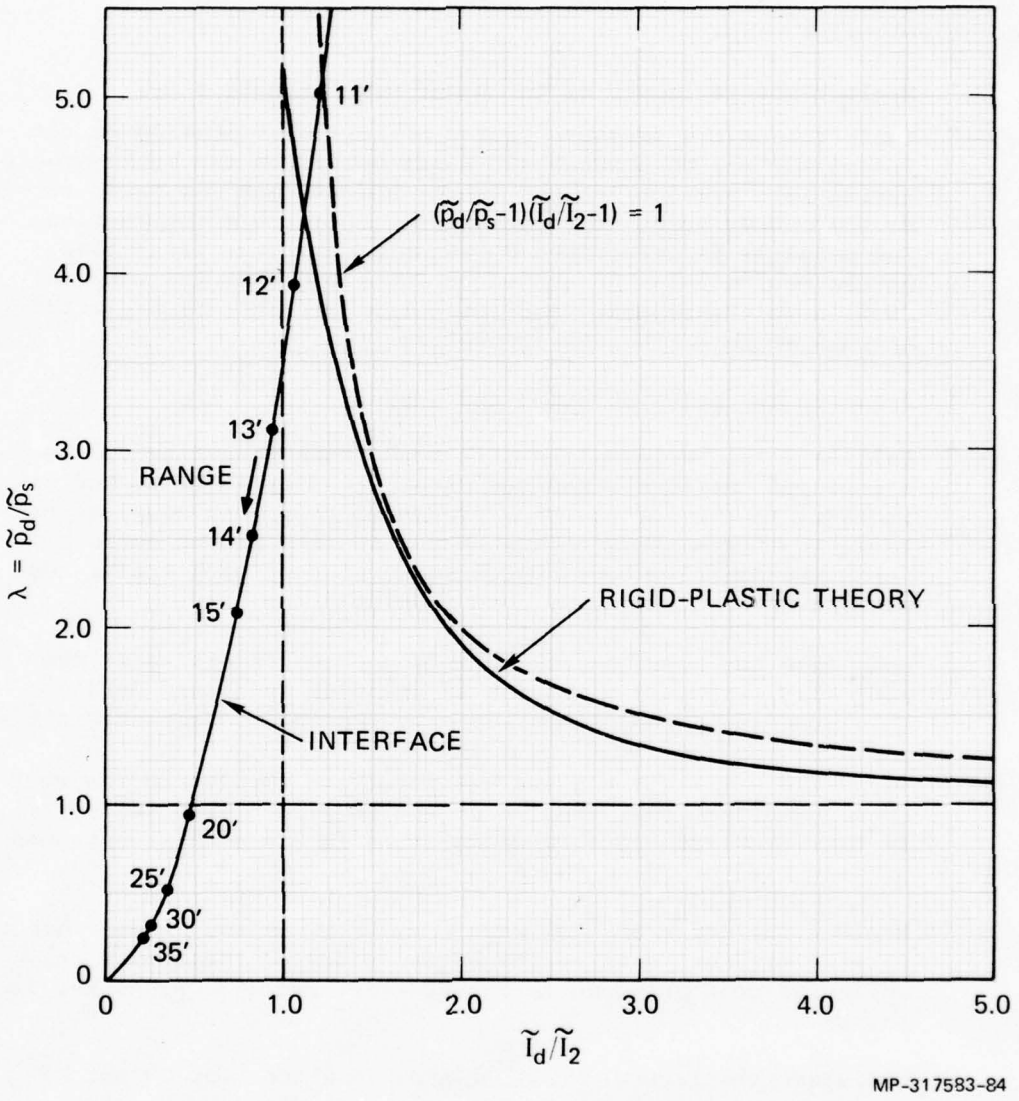

FIGURE 12 PI DIAGRAM FOR BUNKER AND SURFACE LOADING

SUMMARY OF PROCEDURE

The procedure developed above for obtaining the PI characterization of a shallow-buried box bunker subjected to a surface blast wave consists of the following steps:

- Neglect the influence of the blast wave transit time.
- Redistribute the pressure from a uniform distribution on the ground surface to a parabolic distribution on the bunker roof, having zero pressure at the center and the maximum pressure at the bunker edges to represent soil-structure interaction. The parabola is determined by assuming that the total load on the roof equals the ground surface load over the roof. (Soil wave transmission and reflection effects are neglected at this stage of the development.)
- Preserve the pulse duration and shape.
- Calculate the average interface peak pressure acting on the entire roof using the assumed parabolic distribution, and set it equal to the surface peak pressure; this step equates the total interface force on the bunker and the ground surface force immediately above, which is consistent with static test and static finite-element code results.
- Calculate the average peak interface pressure acting on the roof slab (internal dimension is the slab span) and define this pressure as the interface pressure for PI characterization.
- Calculate similarly the average interface impulse on the roof span and define this impulse as the interface impulse for PI characterization; this calculation is based on the assumed preservation of pulse shape.
- Neglect influence of soil wave transit times and assume that the lateral pressure acts on the entire sides of the bunker only while the roof pressure is acting (roof and side pressures in phase).
- Calculate the lateral pressure and hence the roof thrust by applying the Mohr-Coulomb criterion with the low cohesion value neglected and using the surface pressure for the vertical stress; for this step, the soil friction angle is required. It is assumed that the total lateral load from the interaction pressure is the same as the lateral load away from the bunker walls, where the pressure distribution is uniform (because of neglect of wave transit).

- Derive the moment-thrust yield condition for the reinforced concrete roof slab design; the yield condition includes the extremes of fully plastic moment and fully plastic thrust.

- Calculate the roof thrust corresponding to the peak surface pressure, divide it by the fully plastic thrust, and determine the ratio of the resistive moment to the fully plastic moment from the yield condition; hence, determine the resistive moment.

- Assume that the roof is a clamped rigid-plastic beam.

- Calculate the average static collapse pressure for the same parabolic distribution as for dynamic loadings; define this pressure as the static collapse pressure required in the PI characterization.

- Replace loading pulse shape by a rectangular pulse having the same peak pressure and impulse. (An impulse reduction is possible if the motion duration turns out to be less than the pulse duration.)

- Calculate the final central deflection from the results of the dynamic rigid-plastic theory (available for rectangular pulses with pressures over five times the static collapse pressure).

- Calculate the static collapse pressure and an approximate ideal impulse for P_o and I_o in the PI characterization.

- Derive the structural PI curve (see Section 3).

- Using P_o and I_o plot the interface PI curve with range as an intrinsic coordinate.

4. BURIED CHARGE LOADING

PROCEDURE

We have used a procedure similar to that described in Section 2 to obtain a Pressure-Impulse (PI) characterization of the WES shallow-buried box bunkers subjected to loading from buried charges. Figure 2 (Section 1) shows the experimental configuration.

The procedure adopted includes the following steps:

- Generate the interface pressure and impulse values from formulas that fit the WES measurements.
- Model the bunker panel next to the buried charge as a clamped rigid-plastic beam.
- Assume that the pressure distribution along the beam is parabolic with zero pressure at the center; define the average pressure as the interaction pressure for PI characterization.
- Neglect thrust because of the proximity of the ground free surface.
- Determine theoretically the static collapse pressure, P_o , of a clamped rigid-plastic beam with the parabolic pressure distribution.
- Substitute the results P_1, I_1 of the WES incipient failure experiment and the static collapse pressure P_o in formula (2) to determine the ideal impulse I_o
- Plot the universal PI curve given by formula (1); this curve will pass through the points P_1, I_1.
- Plot the interface PI curve with range as an intrinsic coordinate.

More experimental data and at least a simple theoretical treatment for buried charges are required to establish whether the resulting PI characterization can be used to predict failure loads for other bunker designs, soils, and explosive weights.

PI CHARACTERIZATION

Free field pressures and impulses from buried spherical charges may be approximated by formulas of the form

$$P = k_p \lambda^{-n} \qquad I = k_i \lambda^{-m} \qquad \lambda = R/W^{1/3} \tag{14}$$

with R as the range and W as the explosive weight. Empirical fits of the WES data are

$$P = 2650\lambda^{-4.98} \text{ psi} \qquad I = 3202\lambda^{-2.77} \text{ psi-ms} \tag{15}$$

For the incident pulse where, in λ, the range R is given in feet and the TNT explosive weight W is given as 21 lb. Fits of the interface pressure and impulse measurements are

$$P = 2800\lambda^{-2.45} \text{ psi} \qquad I = 4444\lambda^{-1.13} \text{ psi-ms} \tag{16}$$

The parabolic distribution of pressure, Eq. (5), with zero central pressure, is taken to represent the soil-structure interaction. The fully plastic moment without thrust is M_o; hence, the average pressure required to cause static collapse is

$$P_o = \frac{8M_o}{\ell^2}$$

where the beam span is 2ℓ.

In the WES experiment the box bunkers were twice the size of the one shown in Figure 5. Hence, the results in Section 3 give the fully plastic moment as

$$M_o = 16{,}400 \text{ lb. in./in.}$$

so that Eq. (17) gives the static collapse pressure as

$$P_o = 228 \text{ psi}$$

In the WES experiments incipient structural failure occurred when the range was 4 feet, and catastrophic failure occurred when the range was 2-3/4 feet. These results are shown schematically in Figure 13. According to Eq. (16), the interface pressure and impulse values at a range of 4 feet are

$$P_1 = 1127 \text{ psi} \qquad I_1 = 2920 \text{ psi-ms}$$

These values and the static collapse pressure substituted in Eq. (2) give

$$I_o = 2329 \text{ psi-ms}$$

Thus the universal structural PI curve can be determined and plotted as shown in Figure 14.

Elimination of λ from Eq. (16) and introduction of P_o and I_o give the interaction PI curve

$$\frac{P}{P_o} = 3.02 \left(\frac{I}{I_o}\right)^{2.17}$$

This curve is also plotted in Figure

Figure 14 is the required PI characterization of the box bunkers. As indicated above, further research is necessary to establish whether the characterization can be generalized. For example, the procedure for determining the effects of other explosive weights is simply to note that $\lambda = R/W^{1/3} = 1.45$ (R = 4 feet, W = 2 lb TNT) at incipient failure so $R = \lambda W^{1/3}$ gives the new range. However, for larger charges the interface PI curve may not be the same because of the influence of the free surface.

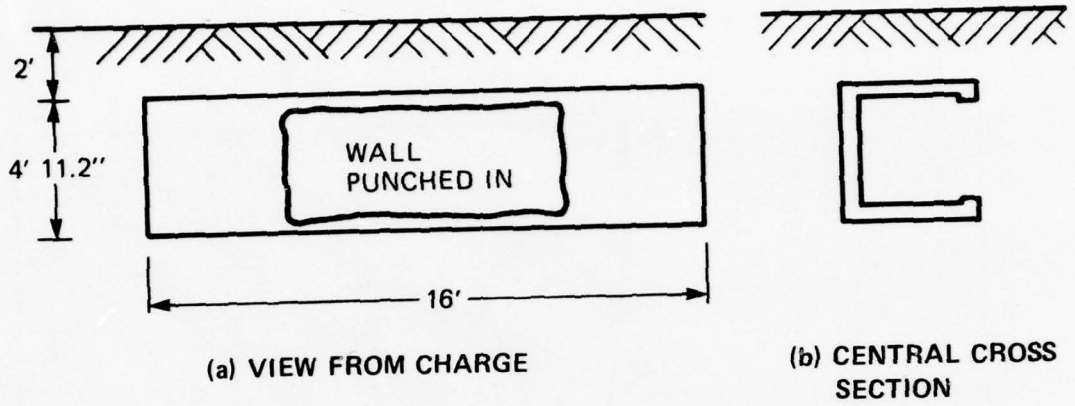

FIGURE 13 BOX BUNKER DAMAGE FROM 21-POUND TNT BURST AT 2-3/4-FOOT AND 4-FOOT RANGES

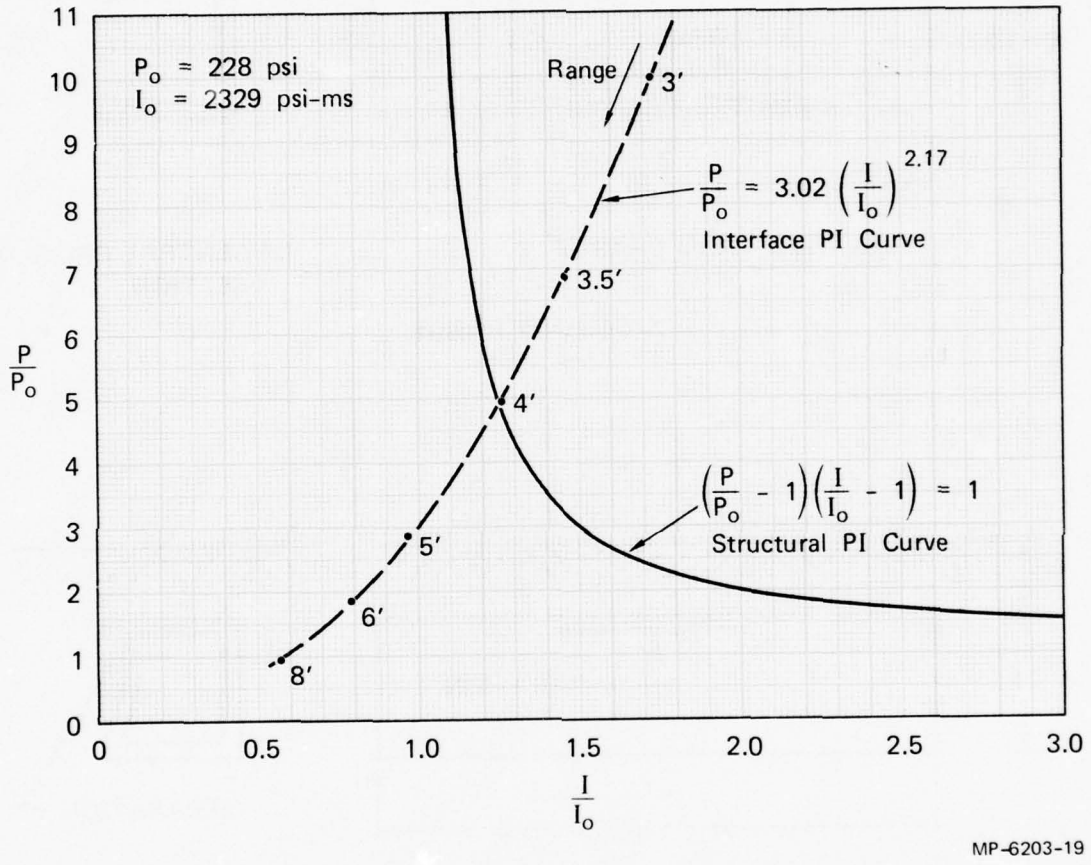

FIGURE 14 PI DIAGRAM FOR BUNKER AND BURIED CHARGE

Appendix A

RESPONSE OF A CLAMPED BEAM TO A SYMMETRICALLY DISTRIBUTED RECTANGULAR PULSE

INTRODUCTION

The purpose of this analysis is to determine the permanent contral deflection of a clamped beam caused by a rectangular pulse that is symmetrically distributed about the center. Because we are investigating structural failure, the deflections are much larger than elastic deflections. Consequently, the material behavior may be considered rigid-perfectly plastic. The choice of a rectangular pulse greatly simplifies the analy sis and should cause deflections similar to those caused by a blast pulse when the duration and blast characteristic time are a fraction of the structural response time. The symmetrical pressure distribution is an approximate representation of soil-structure interaction and is specialized to a parabolic distribution having the minimum pressure at the center.

The beam supports are allowed to approach each other so that negligible tensile membrane forces develop. Also, while the pressure pulse is acting it is assumed that a constant thrust is applied, having as its only effect the creation of an increased fully plastic resistive moment in the beam. When the pressure pulse ends, the thrust also ends.

In rigid-plastic theory, the pulse pressure must exceed the static collapse pressure to produce permanent deformation. The static and dynamic pressures therefore differ in magnitude, but the distributions are chosen to be the same.

STATIC COLLAPSE PRESSURE

As the static pressure $p(x)$ is increased, plastic hinges appear at the center and at the supports to form the static collapse mechanism (Figure A1). At each hinge, the fully plastic moment is M_s and the equation of equilibrium at incipient collapse is

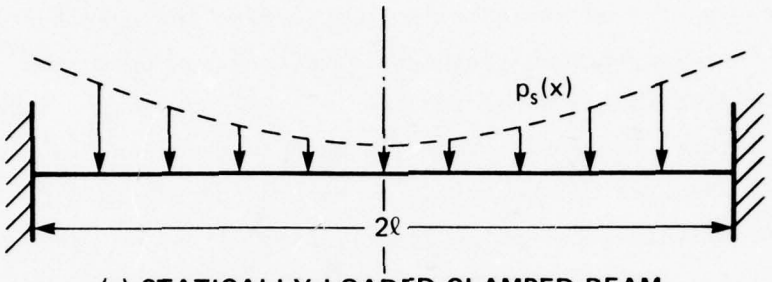

(a) STATICALLY LOADED CLAMPED BEAM

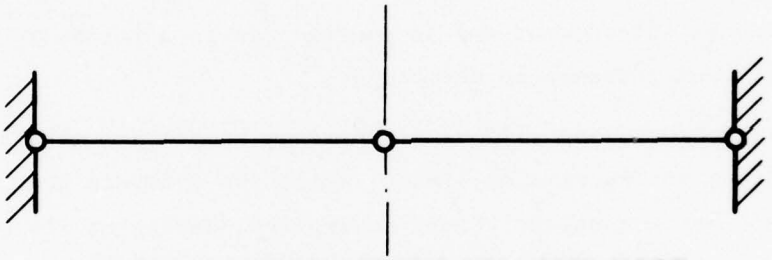

(b) THREE-HINGED STATIC COLLAPSE MODE

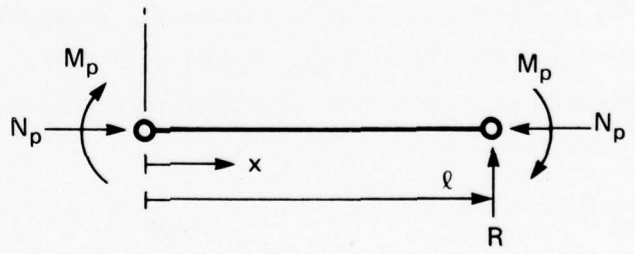

(c) FORCES AND MOMENTS

MA-6203-1

FIGURE A1 STATIC COLLAPSE OF A RIGID-PLASTIC CLAMPED BEAM

$$F_s(\ell) = 2\, M_s \tag{A1}$$

where

$$F_s(\ell) = \int_0^{\ell} (\ell - x)\, p_s(x)\, dx \tag{A2}$$

A parabolic distribution of pressure is described by

$$p_s = q_o + q_2 \frac{x^2}{\ell^2} \tag{A3}$$

so the average pressure $\tilde{p}_s$ and $F_s(\ell)$ from (A2) are

$$\tilde{p}_s = q_o + \frac{1}{3} q_2 \tag{A4}$$

$$F_s(\ell) = \frac{1}{2} \left(q_o + \frac{1}{6} q_2 \right) \ell^2 \tag{A5}$$

and the equilibrium equation (A1) becomes

$$q_o + \frac{1}{6} q_2 = \frac{4\, M_s}{\ell^2} \,. \tag{A6}$$

For zero central pressure we have $q_o = 0$; hence, Eqs. (A4) and (A6) give the static collapse pressure

$$\tilde{p}_s = \frac{8\, M_s}{\ell^2} \tag{A7}$$

DYNAMIC RESPONSE IN MECHANISM 1

If the suddenly applied pressure is only slightly greater than the static collapse pressure, it is reasonable to postulate that the beam will deform in the static collapse mode because the inertial forces are not large enough to affect the mechanism. Consequently, the displacement field is taken as

$$w = W \left(1 - \frac{x}{\ell} \right)$$

where W(t) is the central deflection.

In the notation of Figure A2, the equations of motion are

$$\frac{\partial Q}{\partial x} = -p + \mu \frac{\partial^2 w}{\partial t^2} \qquad Q = \frac{\partial M}{\partial x} \tag{A9}$$

when rotary inertia is neglected.

We analyze the motion in two phases. Phase 1 is the initial loaded phase and Phase 2 is the subsequent unloaded phase.

Phase 1 $\quad p = p_d(x), \; t < t_d$

When we substitute the displacement field (A8) in Eqs. (A9), integrate spatially, and use the hinge conditions $M(o) = M_d$ and $M(\ell) = -M_d$, we obtain the governing equation

$$\ddot{W} = \frac{3}{\mu \ell^2} \left[F_d(\ell) - 2 M_d \right] \tag{A10}$$

where

$$F_d(\ell) = \int_o^\ell (\ell - x) \, p_d(x) \, dx \tag{A11}$$

Dots over symbols indicate time differentiation.

We introduce a pressure parameter defined by

$$\lambda = \frac{p_d(x)}{p_s(x)} \tag{A12}$$

so that from Eqs. (A1), (A2), and (A11) we have

$$F_d(\ell) = \lambda F_s(\ell) = 2 M_s \lambda \tag{A13}$$

Eq. (A10) may therefore be written in the form

$$\ddot{W} = \frac{6M_o}{\mu \ell^2} (\lambda m_s - m_d) \tag{A14}$$

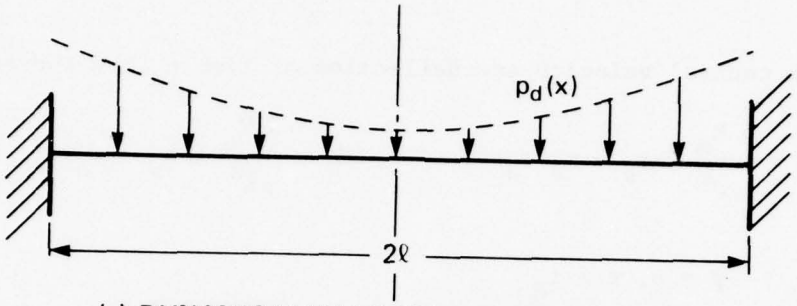

(a) DYNAMICALLY LOADED CLAMPED BEAM

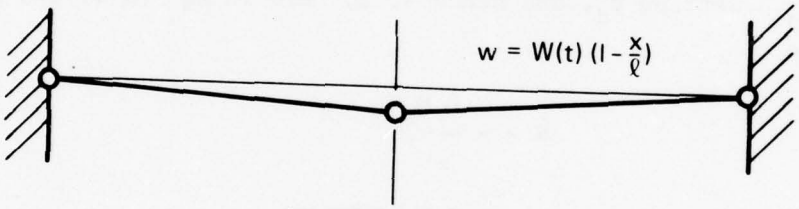

(b) MECHANISM 1

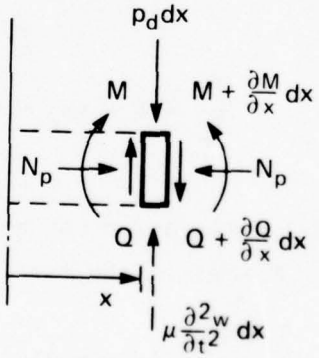

(c) FORCES AND MOMENTS ON RIGID BEAM ELEMENT

MA-6203-3

FIGURE A2 DYNAMIC COLLAPSE OF A RIGID-PLASTIC CLAMPED BEAM

where

$$m_s = \frac{M_s}{M_o} \qquad m_d = \frac{M_d}{M_o} \tag{A15}$$

The beam central velocity and deflection at time t_d are therefore

$$\dot{W}_d = \frac{6\,M_o}{\mu \ell^2}(\lambda m_s - m_d)t_d \qquad W_d = \frac{3\,M_o}{\mu \ell^2}(\lambda m_s - m_d)t_d^2 \tag{A16}$$

Phase 2 $\quad p = o,\ t > t_d$

We assume that in this phase the thrust is no longer acting, so that the fully plastic moment decreases instantaneously at time t_d from M_d to M_o. Setting p_d, and hence λ, to zero in Eq. (A14) and replacing M_d by M_o give

$$\ddot{W} = -\frac{6\,M_o}{\mu \ell^2} \tag{A17}$$

Temporal integration of Eq. (A17), substitution of the initial velocity condition (A16), and setting $\dot{W}(f_f) = 0$ lead to the equation for the duration of motion t_f,

$$\frac{t_f}{f_d} = 1 + \lambda m_s - m_d \tag{A18}$$

Another temporal integration and substitution of the initial displacement condition (A16) gives the final central deflection as

$$W_f = \frac{3\,M_o t_d^2}{\mu \ell^2}(\lambda m_s - m_d)(1 + \lambda m_s - m_d) \tag{A19}$$

For a parabolic pressure distribution with zero central pressure we have the average pressure

$$\tilde{p}_d = \lambda \tilde{p}_s = \frac{8\ M_o}{\ell^2} \cdot \lambda m_s \tag{A20}$$

so that formula (A19) for the final central deflection becomes

$$W_f = \frac{3\ \tilde{p}_d t_d^2}{8\mu} \left(1 - \frac{m_d}{\lambda m_s}\right)\ (1 + \lambda m_s - m_d) \tag{A21}$$

Pressure Limit

Pressures considerably higher than the static collapse pressure initiate mechanisms different from mechanism 1 because of the greater importance of the inertial forces. The upper limit of $\tilde{p}_d$ or λ to initiate mechanism 1 is determined by a change of sign at a central or support plastic hinge of the second spatial derivative of the moment because this implies incipient violation of the yield condition. From Eqs. (A9)

$$\frac{\partial^2 M}{\partial x^2} = -p_d + \mu \frac{\partial^2 W}{\partial t^2} \tag{A22}$$

After substituting the displacement field (A8) in (A22) and setting in turn the hinge locations $x = o$ and $x = \ell$, we see that the upper limit of λ is obtained by a sign change at the center. This limit for zero central pressure is $\lambda_1 = 1$; hence, mechanism 1 cannot be initiated by this special parabolic distribution of pressure.

DYNAMIC RESPONSE IN MECHANISM 2

For load parameters slightly higher than λ_1 the beam responds in mechanism 2 (Figure A3), which has four plastic hinges. While the rectangular pulse is acting, the hinges remain stationary at $x = \bar{x}_1$ and the central portion of the beam moves by rigid body translation.

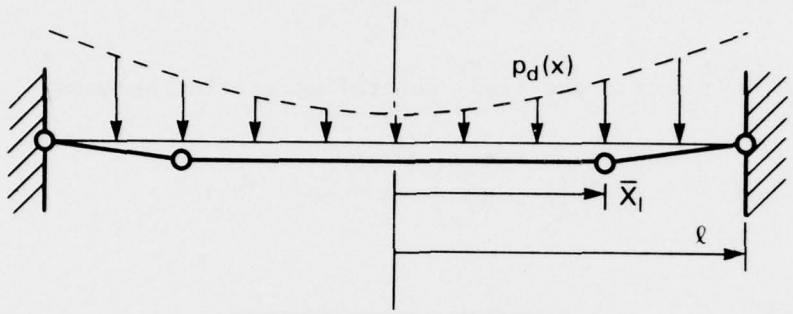

(a) MECHANISM 2. PHASE 1

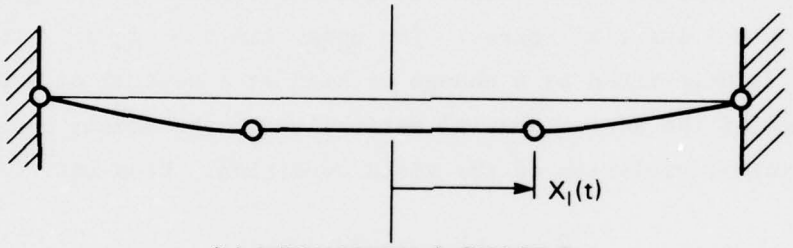

(b) MECHANISM 2. PHASE 2

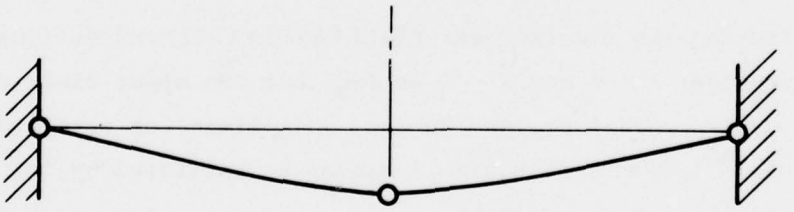

(c) MECHANISM 1. PHASE 3

MA-6203-2

FIGURE A3 DYNAMIC RESPONSE BY INITIAL MECHANISM 2

Phase 1 $$p = p_d(x), \quad t < t_d \tag{A23}$$

While the constant pressure is acting the displacement field is

$$w = \begin{cases} W & o \le x \le \bar{x}_1 \\ W \dfrac{\ell - x}{\ell - \bar{x}} & \bar{x}_1 \le x \le \ell \end{cases}$$

Substitution of $w = W$ for $o \le x \le \bar{x}_1$ in the equations of motion (A9), spatial integration, and application of the conditions $Q(\bar{x}_1) = 0$ and $M(\bar{x}_1) = M_d$, give

$$\ddot{W} = \frac{\bar{p}_d}{\mu} \tag{A24}$$

$$M(o) = M_p + F_d\left(\bar{x}_1\right) - \bar{x}_1\left(\ell - \frac{\bar{x}_1}{2}\right)\bar{p}_d \tag{A25}$$

where

$$\bar{p}_d = \frac{1}{\bar{x}_1}\int_o^{\bar{x}_1} p_d(x)\, dx \tag{A26}$$

$$F_d(\bar{x}_1) = \int_o^{\bar{x}_1} (\ell - x)\, p_d(x)\, dx \tag{A27}$$

Substitution of the displacement field (A23) for $\bar{x}_1 \le x \le \ell$ in the equations of motion (A9), spatial integration, and application of the conditions $M(\bar{x}_1) = M_d$ and $M(\ell) = -M_d$, give

$$2\, M_d = F_d(\ell) - F_d\left(\bar{x}_1\right) - \frac{1}{3}\left(\ell - \bar{x}_1\right)^2 \bar{p}_d \tag{A28}$$

The unknowns in Eqs. (A24), (A25), and (A28) are the central deflection W, the central moment M(o), and the hinge location $\bar{x}_1$. The hinge location can be determined from Eq. (A28). For the parabolic pressure distribution (A3) with $q_o = 0$, Eq. (A28) reduces to

$$\left(1 - \bar{\rho}_1\right)^2\left(3 + 6\bar{\rho}_1 + 5\bar{\rho}_1^2\right) = 3m_d/\lambda m_s \tag{A29}$$

From Eq. (A24) the central velocity and deflection at time t_d are

$$\dot{W}_d = \frac{\bar{P}_d t_d}{\mu} \qquad W_d = \frac{\bar{P}_d t_d^2}{2\mu} \tag{A30}$$

where, for zero central pressure

$$\bar{P}_d = \lambda \bar{P}_s = \frac{8 M_s}{\ell^2} \lambda \bar{\rho}_1 \tag{A31}$$

Phase 2 $\qquad p = 0, \; t_1 < t < t_c$

After the pressure has been applied, the hinges travel toward the center of the beam; let the arrival time be t_c. The velocity field corresponding to this phase of deformation is

$$\frac{\partial w}{\partial t} = \begin{cases} V & 0 \le x \le x_1(t) \\ V \dfrac{\ell - x}{\ell - x_1} & x_1(t) \le x \le \ell \end{cases} \tag{A32}$$

where $V = V(t)$ is the velocity of the center of the beam.

In the region $0 < x < x_1(t)$, the velocity field (A32), the equations of motion (A9), and initial conditions (A30), give at time t_c

$$V_c = \dot{W}_c = \dot{W}_d \qquad W_c = \dot{W}_d + W_d \, (t - t_d) \tag{A33}$$

In the region $x_1(t) < x < \ell$, the velocity field (A32), the equations of motion (A9), initial conditions (A30), and moment conditions $M(x_1) = M_o$ and $M(\ell) = -M_o$, give at time t_c

$$t_c - t_d = \frac{\mu V_c}{12 M_o} \left[\ell^2 - \left(\ell - \bar{x}_1 \right)^2 \right] \tag{A34}$$

Phase 3 $\quad p = 0,\ t_c < t < t_f$

The remaining deformation occurs in mechanism 1, which is the static collapse mode, and has the velocity field

$$\frac{\partial w}{\partial t} = V\left(1 - \frac{x}{\ell}\right) \qquad 0 \le x \le \ell \tag{A35}$$

The initial conditions of this phase are Eqs. (A33). The solution of the equations of motion (A9) with velocity field (A35) and initial conditions is

$$W_f - W_c = \frac{1}{2} V_c\left(t_f - t_c\right) \tag{A36}$$

$$t_f - t_c = \frac{\mu V_c \ell^2}{6 M_o} \tag{A37}$$

where W_f is the required final central deflection and t_f is the duration of motion. Explicitly, the final central deflection is

$$W_f = \frac{\bar{p}_d t_d^2}{2\mu}\left\{1 + \frac{\bar{p}_d \ell^2}{6 M_o}\left[2 - \left(1 - \bar{\rho}_1\right)^2\right]\right\} \tag{A38}$$

For the parabolic pressure distribution (A3) with $q_o = 0$, the initial hinge location $\bar{\rho}_1$ is the solution of Eq. (A29), and the central deflection is

$$W_f = \frac{\tilde{p}_d t_d^2}{2\mu}\,\bar{\rho}_1^2\left\{1 + \frac{4}{3} m_s \bar{\rho}_1^2\left[2 - \left(1 - \bar{\rho}_1\right)^2\right]\right\} \tag{A39}$$

and the duration of motion is given by

$$\frac{t_f}{t_d} = 1 + \frac{2}{3} m_s \bar{\rho}_1^2\left[3 - \left(1 - \rho_1\right)^2\right] \tag{A40}$$

Pressure Limit

Mechanism 2 requires that the central bending moment lie in the range $-M_d < M(o) < M_d$. The largest value of λ that allows this condition to be satisfied is determined by Eq. (A25) with $M(o) = -M_d$, that is,

$$\lambda_2 \left[\bar{x}_1 \left(\ell - \frac{\bar{x}_1}{2} \right) \bar{p}_s - F_s(\bar{x}_1) \right] = 2 M_d \qquad \text{(A41)}$$

For a parabolic pressure distribution with zero central pressure, formula (A41) gives

$$\frac{\lambda_2 m_s}{m_d} = \frac{1}{\bar{\rho}_1^4} \qquad \text{(A42)}$$

and Eq. (A29) determines ρ_1 by becoming

$$3 \bar{\rho}_1^{-4} - \left(1 - \bar{\rho}_1\right)^2 \left(3 + 6 \bar{\rho}_1 + 5 \bar{\rho}_1\right) = 0 \qquad \text{(A43)}$$

Thus, to find λ_2, we solve Eq. (A43) for $\bar{\rho}_1$ and substitute in Eq. (A42). Calculations show that $\bar{\rho}_1 = 0.72$ and $\lambda_2 = 5.27$. The pressure limit for activating mechanism 2 is therefore over five times the static collapse pressure.

Appendix B

REINFORCED CONCRETE BEAM YIELD CONDITION

INTRODUCTION

This appendix outlines the derivation of the yield condition for the reinforced concrete slabs of the box bunker. The yield condition is a relationship between the bending moment M and the axial thrust N when the cross section yields plastically over its entire surface. In the derivation the following assumptions are required:

- Plane sections remain plane during deformation
- Perfect bonding exists between the steel and concrete
- The steel is perfectly plastic (no hardening)
- The concrete is perfectly plastic in compression and has no tensile strength
- Round reinforcing bars may be approximated by square ones

MOMENT AND THRUST FORMULAS

Figure B1 shows the geometrical nomenclature of the slab; the usual round bars have been replaced by square ones having the same area for algebraical convenience only. Figure B2 shows the four stress distributions that can arise for the bunker slab cross section. Figure B2a applies when the neutral axis (plane of zero strain) at depth c intersects the upper steel, that is, when $d_1' < c < d_2'$. For the properties of the bunker slab, the limiting conditions of zero thrust and fully plastic moment M_o fall in this case. As the thrust is increased and the moment is changed to keep the section fully plastic, the depth of the neutral axis increases, resulting in the stress distributions of Figures B2b, c, and d. The limiting condition is the fully plastic

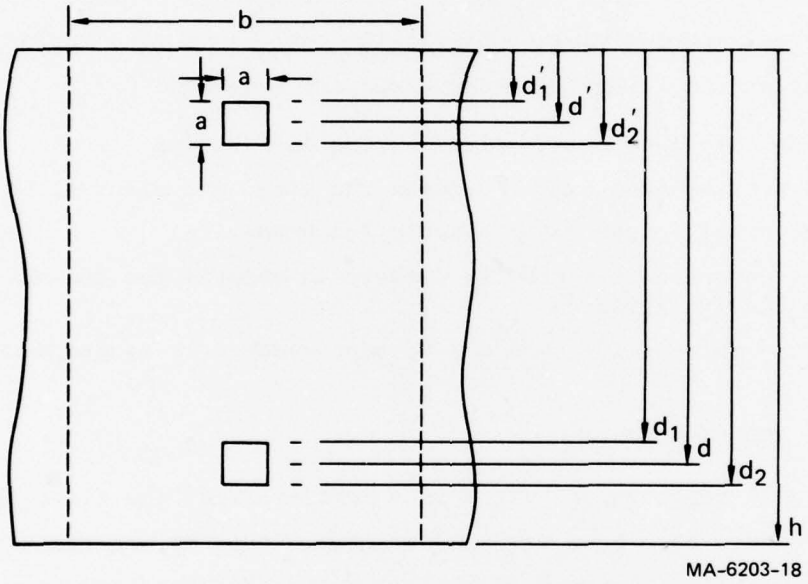

FIGURE B1 SLAB GEOMETRICAL NOMENCLATURE

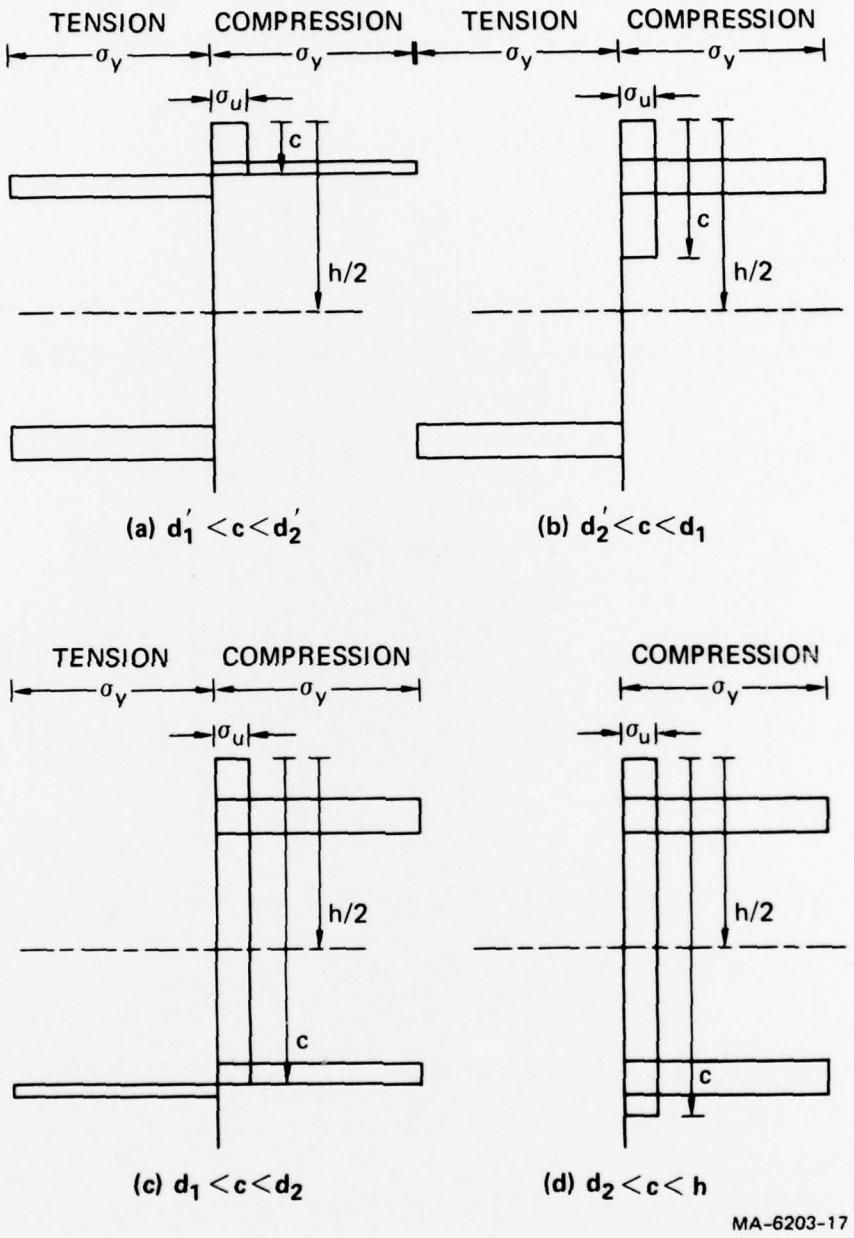

FIGURE B2 STRESS DISTRIBUTIONS ON FULLY PLASTIC CROSS SECTION

thrust N_o with no resistive moment. Formulas for the moments and thrusts are derived below for the four cases in Figure B2. Dimensionless quantities that are convenient for expressing results are

$$\alpha = \frac{a^2}{bh} \qquad \beta = \frac{a}{b} \qquad \gamma = \frac{c}{h} \qquad \delta = \frac{d}{h} \qquad S = \frac{\sigma_y}{\sigma_u} \tag{B1}$$

Case 1: $d_1 < c < d_2$

The stress distribution in Figure B2a may be represented by the following forces and corresponding moments (moments about section mid-height):

$$N_c' = bc\sigma_u \qquad M_c' = N_c'\left(\frac{h}{2} - \frac{c}{2}\right)$$

$$\bar{N}_c' = a\left(c - d_1'\right)\sigma_u \qquad \bar{M}_c' = \bar{N}_c'\left[\frac{h}{2} - \frac{1}{2}\left(d_1' + c\right)\right]$$

$$N_{su} = a\left(c - d_1'\right)\sigma_y \qquad M_{su}' = N_{su}\left[\frac{h}{2} - \frac{1}{2}\left(d_1' + c\right)\right]$$

$$N_{s1}' = a\left(d_2' - c\right)\sigma_y \qquad M_{s1}' = N_{s1}'\left[\frac{h}{2} - \frac{1}{2}\left(c + d_2'\right)\right]$$

$$N_s = a^2\sigma_y \qquad M_s = N_s\left(d - \frac{h}{2}\right)$$

The compressive axial force and the binding moment are

$$N = N_c' - \bar{N}_c' + N_{su} - N_{s1}' - N_s$$

$$M = M_c' - \bar{M}_c' + M_{su}' - M_{s1}' + M_s$$

Hence

$$\frac{N}{bh\sigma_u} = \gamma + (s - 1)\beta\left(\gamma - \delta_1'\right) - s\beta\left(\delta_2' - \gamma\right) - s\alpha \tag{B2}$$

$$\frac{2M}{bh^2\sigma_u} = \gamma(1-\gamma) + (s-1)\beta\left(\gamma - \delta_1'\right)\left[1-\left(\gamma + \delta_1'\right)\right] - s\beta\left(\delta_2' - \gamma\right)\left[1 - \left(\gamma + \delta_2'\right)\right] + s\alpha\left(1 - 2\delta'\right) \quad \text{(B3)}$$

If we set N=o in (B2) we obtain $\gamma = \gamma_o$ where

$$\gamma_o = \frac{(2s-1)\beta\,\delta' + (2s+1)\alpha}{2[1+(2s-1)\beta]} \quad \text{(B4)}$$

which gives the position of the neutral axis for bending alone provided $\delta_1' < \gamma_o < \delta_2'$. For the bunker design of Figure B2a this inequality is satisfied. Thus, setting $\gamma = \gamma_o$ in Eq. (B3) gives the fully plastic moment M_o without thrust.

Case 2: $d_2' < c < d_1$

The stress distribution in Figure B2b may be represented by the following forces and corresponding moments:

$$N_c' = bc\sigma_u \qquad M_c' = N_c'\left(\frac{h}{2} - \frac{c}{2}\right)$$

$$\overline{N}_c' = a^2\sigma_u \qquad \overline{M}_c' = \overline{N}_c'\left(\frac{h}{2} - d'\right)$$

$$N_s' = a^2\sigma_y \qquad M_s' = N_s'\left(\frac{h}{2} - d'\right)$$

$$N_s = a^2\sigma_y \qquad M_s = N_s\left(d - \frac{h}{2}\right)$$

The compressive axial force and bending moment are

$$N = N_c' - \overline{N}_c' + N_s' - N_s$$

$$M = M_c' - \overline{M}_c' + M_s' + M_s$$

Hence,

$$\frac{N}{bh\sigma_u} = \gamma - \alpha \quad \text{(B5)}$$

$$\frac{2M}{bh^2\sigma_u} = \gamma\,(1 - \gamma) + (2s - 1)\,\alpha\,(1 - 2\delta') \qquad \text{(B6)}$$

Case 3: $d_1 < c < d_2$

The stress distribution in Figure B2c may be represented by the following forces and corresponding moments:

$$N'_c = bc\,\sigma_u \qquad M'_c = N'_c\left(\frac{h}{2} - \frac{c}{2}\right)$$

$$N'_c = a^2\sigma_u \qquad \bar{M}'_c = \bar{N}'_c\left(\frac{h}{2} - d'\right)$$

$$N'_s = a^2\sigma_y \qquad M'_s = N'_s\left(\frac{h}{2} - d'\right)$$

$$N_{su} = a\,(c - d_1)\sigma_y \qquad M_{su} = N_{su}\left[\tfrac{1}{2}(c + d_1) - \frac{h}{2}\right]$$

$$N_{sl} = a(d_2 - c)\sigma_y \qquad M_{sl} = N_{sl}\left[\tfrac{1}{2}(c + d_2) - \frac{h}{2}\right]$$

$$N_{cu} = a(c - d_1)\sigma_u \qquad \bar{M}_{cu} = \bar{N}_{cu}\left[\tfrac{1}{2}(c + d_1) - \frac{h}{2}\right]$$

The compressive axial force and bending moment are

$$N = N'_c - \bar{N}'_c + N'_s + N_{su} - N_{sl} - \bar{N}_{cu}$$

$$M = M'_c - \bar{M}'_c + M'_s - M_{su} + M_{sl} + \bar{M}_{cu}$$

Hence,

$$\frac{N}{bh\sigma_u} = \gamma + (s - 1)\,\beta\,(\gamma - \delta_1) - s\beta\,(\delta_2 - \gamma) + (s - 1)\alpha \qquad \text{(B7)}$$

$$\frac{2M}{bh^2\sigma_u} = \gamma\,(1 - \gamma) - (s - 1)\beta\,(\gamma - \delta_1)\left[(\gamma - \delta_1) - 1\right] + s\beta\,(\delta_2 - \gamma)\left[(\gamma + \delta_2) - 1\right] + (s - 1)\alpha\,(1 - 2\delta') \qquad \text{(B8)}$$

Case 4: $d_2 < c < h$

The stress distribution in Figure B2d may be represented by the following forces and corresponding moments:

$$N_c' = bc\sigma_u \qquad M_c' = N_c\left(\frac{h}{2} - \frac{c}{2}\right)$$

$$\overline{N}_c' = a^2\sigma_u \qquad \overline{M}_c' = N_c'\left(\frac{h}{2} - d'\right)$$

$$N_s' = a^2\sigma_y \qquad M_s' = N_s'\left(\frac{h}{2} - d'\right)$$

$$N_s = a^2\sigma_y \qquad M_s = N_s\left(\frac{h}{2} - d'\right)$$

$$\overline{N}_c = a^2\sigma_u \qquad \overline{M}_c = \overline{N}_c\left(\frac{h}{2} - d'\right)$$

The compressive axial force and bending moment are

$$N = N_c' - N_c' + N_s' + N_s - \overline{N}_c$$

$$M = M_c' - \overline{M}_c + M_s' - M_s + \overline{M}_c$$

Hence,

$$\frac{N}{bh\sigma_u} = \gamma + 2(s - 1)\alpha \qquad \text{(B9)}$$

$$\frac{2M}{bh^2\sigma_u} = \gamma\,(1 - \gamma) \qquad \text{(B10)}$$

When $\gamma = 1$, the section sustains only an axial force N_o, which from Eq. (B9) is

$$\frac{N_o}{bh\sigma_u} = 1 + 2\,(s - 1)\alpha \qquad \text{(B11)}$$

Dimensionless forms of the moment and thrust that are convenient for expressing the yield condition are

$$m = M/M_o \qquad n = N/N_o \tag{B12}$$

where M_o and N_o are given by Eq. (B3) with $\gamma = \gamma_o$ and Eq. (B11). The simplest way to construct the yield curve is to regard the dimensionless depth of the neutral axis as a parameter and to call upon the moment and thrust formulas according to the range in which γ falls.

SLAB YIELD CONDITION

Data corresponding to the design in Figure 5 are:

Slab thickness	$h = 2.8$ in
Spacing of reinforcing bars	$b = 2.0$ in
Diameter of reinforcing bars	$D = 1/4$ in
Area of reinforcing bar	$A_s = 0.049$ in^2
Side of equivalent square bar	$a = 0.222$ in
Depth to center of upper steel	$d' = 0.4$ in
Depth to center of lower steel	$d = 2.4$ in
Depth to top of upper square bar	$d_1' = 0.289$ in
Depth to bottom of upper square bar	$d_2' = 0.511$ in
Depth to top of lower square bar	$d_1 = 2.289$ in
Depth to bottom of lower square bar	$d_2 = 2.511$ in
Crush strength of concrete	$\sigma_u = 6{,}000$ psi
Yield strength of steel	$\sigma_y = 72{,}000$ psi

From these data the following parametric values were obtained:

$\alpha = a^2/bh = 0.00877$

$\beta = a/b = 0.111$

$\delta_1' = d_1'/h = 0.103$

$\delta' = d/h = 0.143$

$\delta_2' = d_2'/h = 0.182$

$\delta_1 = d_1/h = 0.818$

$\delta = d/h = 0.857$

$\delta_2 = d_2/h = 0.897$

$s = \sigma_y/\sigma_u = 12$

The resulting fully plastic moment with no thrust, fully plastic thrust with no moment, and the dimensionless depth of the neutral axis when the moment acts alone are

$M_o = 4{,}100$ lb. in/in

$N_o = 20{,}000$ lb/in

$\gamma_o = 0.134 \quad \left(\delta_1' < \gamma_o < \delta_2'\right)$

Table B1 lists the values of m and n generated by means of the parameter γ. Figure B3 is the resulting yield curve. An interesting feature of the curve is that when the thrust is about 41% of the fully plastic thrust N_o, the resistive moment is 2.26 times the fully plastic moment M_o.

Table B1

YIELD CURVE VALUES

γ Range and Formulas	γ	m	n
$\delta_1' < \gamma < \delta_2'$	0.134	1.00	0
	0.14	1.10	0.019
(B2) (B3)	0.16	1.38	0.079
	0.18	1.65	0.138
$\delta_2' < \gamma \delta_1$	0.20	1.74	0.160
	0.30	2.03	0.244
	0.40	2.20	0.328
(B5) (B6)	0.50	2.26	0.412
	0.60	2.20	0.496
	0.70	2.03	0.579
	0.80	1.74	0.663
$\delta_1 < \gamma \delta_2$	0.82	1.65	0.685
	0.84	1.38	0.745
(B7) (B8)	0.86	1.10	0.804
	0.88	0.80	0.863
$\delta_2 < \gamma < 1$	0.90	0.516	0.916
	0.94	0.323	0.950
(B9) (B10)	0.98	0.112	0.983
	1.00	0	1.0

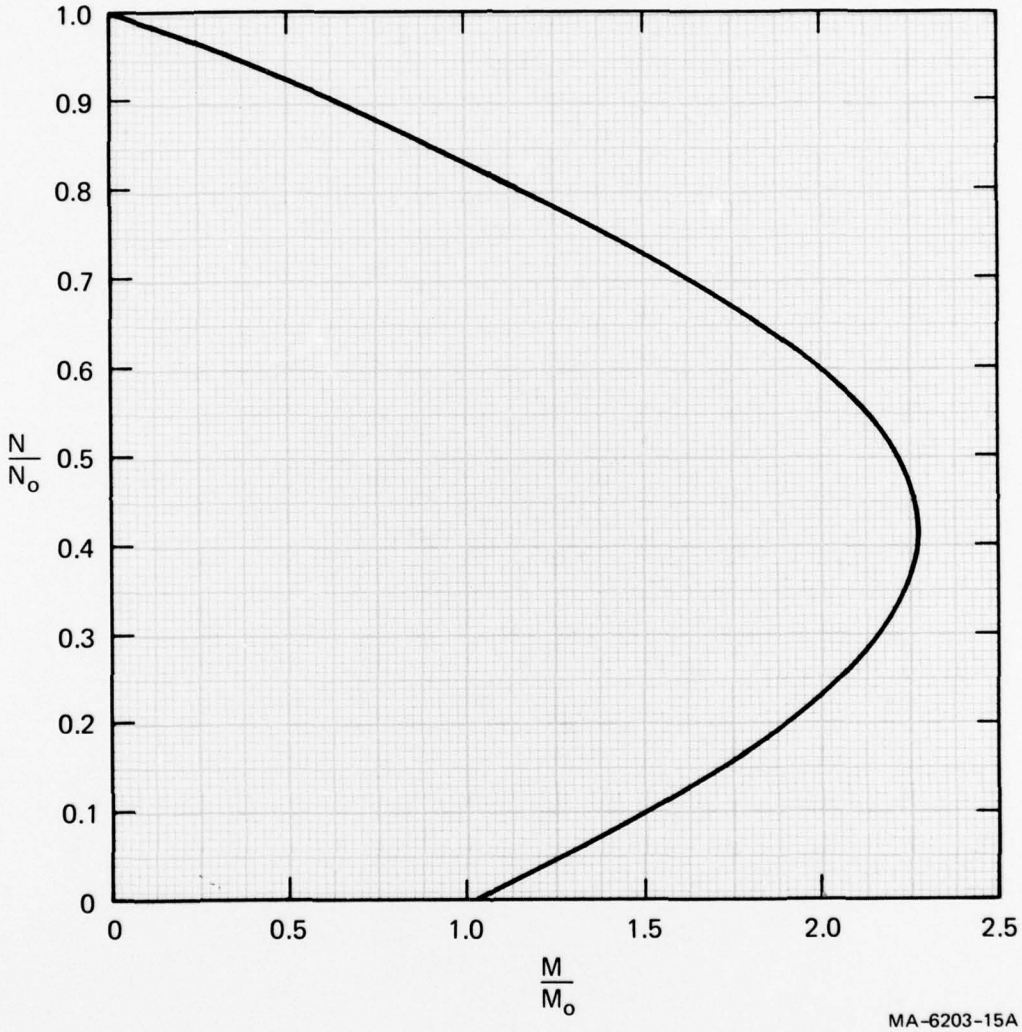

FIGURE B3 MOMENT-THRUST YIELD CONDITION

DISTRIBUTION LIST

DEPARTMENT OF DEFENSE

Assistant to the Secretary of Defense
Atomic Energy
ATTN: ATSD (AE)

Director
Defense Civil Preparedness Agency
Assistant Director for Research
ATTN: G. Sisson

Director
Defense Communications Agency
ATTN: CCTC/C672, F. Moore

Defense Documentation Center
Cameron Station
12 cy ATTN: TC

Director
Defense Intelligence Agency
ATTN: DT-1C
ATTN: DB-4C1
ATTN: DB-4C2, T. Ross
ATTN: DT-2, Wpns. & Sys. Div.

Director
Defense Nuclear Agency
ATTN: STSP
ATTN: SPAS
ATTN: DDST
2 cy ATTN: SPSS
ATTN: TISI
3 cy ATTN: TITL

Commander
Field Command, DNA
ATTN: FCT
ATTN: FCPR

Director
Joint Strat. Tgt. Planning Staff
ATTN: JLTW-2

Chief
Livermore Division, Field Command, DNA
Lawrence Livermore Laboratory
ATTN: FCPRL

Under Secy. of Defense for Rsch. & Engrg.
ATTN: S&SS (OS)

DEPARTMENT OF THE ARMY

Program Manager
BMD Program Office
ATTN: CRDABM-NE

Commander
BMD System Command
ATTN: BDMSC-TEN, N. Hurst

Director
Construction Engineering Rsch. Lab.
ATTN: CERL-SL

DEPARTMENT OF THE ARMY (Continued)

Deputy Chief of Staff for Rsch. Dev. & Acq.
ATTN: DAMA-CSM-N, LTC G. Ogden

Chief of Engineers
ATTN: DAEN-MCE-D
ATTN: DAEN-RDM

Deputy Chief of Staff for Ops. & Plans
ATTN: Dir. of Chem. & Nuc. Ops.

Commander
Harry Diamond Laboratories
ATTN: DELHD-NP

Director
U.S. Army Ballistic Research Labs
ATTN: J. Meszaros
ATTN: J. Keefer
ATTN: C. Kingery

Division Engineer
U.S. Army Engineer Div., Huntsville
ATTN: HNDED-SR

Director
U.S. Army Engr. Waterways Exper. Sta.
ATTN: F. Brown
2 cy ATTN: W. Flathau
2 cy ATTN: G. Jackson

Commander
U.S. Army Foreign Science & Tech. Ctr.
ATTN: Rsch. & Data Branch

DEPARTMENT OF THE NAVY

Chief of Naval Material
ATTN: MAT 0323

Chief of Naval Operations
ATTN: OP 985F

Chief of Naval Research
ATTN: Code 461, J. Warner
ATTN: Code 474, N. Perrone

Officer-in-Charge
Civil Engineering Laboratory
Naval Construction Battalion Center
ATTN: R. Odello
ATTN: L51, W. Shaw
ATTN: J. Crawford

Commander
David W. Taylor Naval Ship R&D Ctr.
ATTN: Code 177, E. Palmer
ATTN: Code 1740.5, B. Whang
ATTN: Code 1700, W. Murray

Commander
Naval Facilities Engineering Command
ATTN: Code 04B
ATTN: Code 03A

DEPARTMENT OF THE NAVY (Continued)

Commander
Naval Ocean Systems Center
ATTN: E. Cooper

Superintendent (Code 1424)
Naval Postgraduate School
ATTN: Code 1424

Director
Naval Research Laboratory
ATTN: Code 8403A, G. O'Hara
ATTN: Code 8440, F. Rosenthal
ATTN: Code 8403, R. Belshem

Commander
Naval Sea Systems Command
ATTN: SEA-9931, R. Lane
ATTN: Code 03511
ATTN: Code 0351

Commander
Naval Ship Engineering Center
ATTN: NSEC 6105

Officer-in-Charge
Naval Surface Weapons Center
ATTN: Code 240
ATTN: Code 241
ATTN: Code 243
ATTN: Code WA501, Navy Nuc. Prgms. Off.

Commander
Naval Surface Weapons Center
Dahlgren Laboratory
ATTN: W. Wisherd

Commander
Naval Weapons Center
ATTN: C. Austin
ATTN: J. Bowen

Commanding Officer
Naval Weapons Evaluation Facility
ATTN: R. Hughes

Director
Strategic Systems Project Office
ATTN: NSP-272

DEPARTMENT OF THE AIR FORCE

Commander
ADCOM/DC
ATTN: KRX

Commander
ADCOM/XPD
ATTN: XPDQQ
ATTN: XPX
ATTN: XP

AF Armament Laboratory, AFSC
ATTN: AFATL/DLYV, J. Collins

AF Institute of Technology, AU
ATTN: Commander

DEPARTMENT OF THE AIR FORCE (Continued)

AF Weapons Laboratory, AFSC
ATTN: DEP
ATTN: DES-S, M. Plamondon
ATTN: DE, Lt Col J. Leech
ATTN: SUL

Headquarters
Air Force Systems Command
ATTN: DLCAW

Commander
Foreign Technology Division, AFSC
ATTN: PDBF, S. Spring

Hq. USAF/RD
ATTN: RDQSM

Commander
Rome Air Development Center, AFSC
ATTN: Commander

SAMSO/DE
ATTN: DEB, MNNH, MNI
ATTN: MMH

Commander in Chief
Strategic Air Command
ATTN: OAI
ATTN: XPFS

DEPARTMENT OF ENERGY

Department of Energy
Albuquerque Operations Office
ATTN: Director

University of California
Lawrence Livermore Laboratory
ATTN: L-96, L. Woodruff
ATTN: L-200, J. Cortez
ATTN: L-200, T. Butkovich

Los Alamos Scientific Laboratory
ATTN: T. Dowler

Sandia Laboratories
ATTN: Doc. Con. for W. Roherty
ATTN: Doc. Con. for L. Vortman
ATTN: Doc. Con. for W. Caudle
ATTN: Doc. Con. for W. Herrmann

OTHER GOVERNMENT AGENCY

Central Intelligence Agency
ATTN: RD/SI, Rm. 5G48, Hq. Bldg. for
NED/OSI-5G48 Hqs.

DEPARTMENT OF DEFENSE CONTRACTORS

Aeropspace Corporation
ATTN: L. Selzer
ATTN: P. Mathur

Agbabian Associates
ATTN: M. Agbabian

Artec Associates, Inc.
ATTN: S. Gill

DEPARTMENT OF DEFENSE CONTRACTORS (Continued)

Battelle Memorial Institute
ATTN: R. Klingesmith

The BDM Corporation
ATTN: A. Lavagnino

The BDM Corporation
ATTN: R. Hensley

Bell Telephone Laboratories
ATTN: J. White

The Boeing Company
ATTN: R. Dyrdahl
ATTN: R. Carlson
ATTN: J. Wooster
ATTN: R. Holmes

Brown Engineering Company, Inc.
Cummings Research Park
ATTN: M. Patel

California Research & Technology, Inc.
ATTN: K. Kreyenhagen
ATTN: S. Shuster

Center for Planning & Rsch., Inc.
ATTN: R. Shnider

Civil/Nuclear Systems Corporation
ATTN: J. Bratton

University of Denver
Colorado Seminary
Denver Research Institute
ATTN: Sec. Officer for J. Wisotski

Electromechanical Sys. of New Mexico, Inc.
ATTN: R. Shunk

Engineering Decision Analysis Co., Inc.
ATTN: R. Kennedy

The Franklin Institute
ATTN: Z. Zudans

Gard, Inc.
ATTN: G. Neidhardt

General Dynamics Corp.
Pomona Division
ATTN: K. Anderson

General Dynamics Corporation
Electric Boat Division
ATTN: M. Pakstys

General Electric Company
Space Division
ATTN: M. Bortner, Space Sci. Lab.

General Electric Company
TEMPO-Center for Advanced Studies
ATTN: DASIAC

H-Tech Laboratories, Inc.
ATTN: B. Hartenbaum

DEPARTMENT OF DEFENSE CONTRACTORS (Continued)

IIT Research Institute
ATTN: R. Robinson
ATTN: A. Longinaw

Institute for Defense Analyses
ATTN: Director

JAYCOR
ATTN: M. McKay

J. H. Wiggins Co., Inc.
ATTN: J. Collins

Kaman AviDyne
Division of Kaman Sciences Corp.
ATTN: N. Hobbs
ATTN: E. Criscione

Kaman Sciences Corporation
ATTN: D. Sachs

Lockheed Missiles and Space Co., Inc.
ATTN: D/52-33, T. Geers, Bldg. 205

Lovelace Foundation for Medical Education & Rsch.
ATTN: Asst. Dir. of Res., R. Jones

Martin Marietta Corporation
Orlando Division
ATTN: G. Fotieo
ATTN: A. Cowen

McDonnell Douglas Corporation
ATTN: R. Halprin
ATTN: J. Logan

Merritt CASES, Inc.
ATTN: J. Merritt

The Mitre Corporation
ATTN: Director

University of New Mexico
Dept. of Campus Security and Police
ATTN: G. Triandafalidis

Nathan M. Newmark
Consulting Engineering Services
ATTN: W. Hall
ATTN: N. Newmark

University of Oklahoma
Research Institute
ATTN: J. Thompson

Pacifica Technology
ATTN: R. Bjork
ATTN: G. Kent
ATTN: R. Allen

Physics International Company
ATTN: D. Orphal
ATTN: L. Behrmann
ATTN: R. Swift
ATTN: E. Moore
ATTN: F. Sauer
ATTN: C. Vincent

DEPARTMENT OF DEFENSE CONTRACTORS (Continued)

R&D Associates
ATTN: H. Cooper
ATTN: C. Knowles
ATTN: H. Brode
ATTN: A. Latter
ATTN: W. Wright, Jr.
ATTN: R. Port
ATTN: J. Lewis
ATTN: J. Carpenter

The Rand Corporation
ATTN: C. Mow
ATTN: A. Laupa

Science Applications, Inc.
ATTN: D. Maxwell

Science Applications, Inc.
ATTN: W. Layson
ATTN: B. Chambers

Science Applications, Inc.
ATTN: H. Wilson

Science Applications, Inc.
ATTN: S. Oston

Southwest Research Institute
ATTN: W. Baker
ATTN: A. Wenzel

SRI International
ATTN: W. Wilkinson
ATTN: G. Abrahamson
ATTN: A. Florence

DEPARTMENT OF DEFENSE CONTRACTORS (Continued)

Systems, Science and Software, Inc.
ATTN: K. Pyatt
ATTN: D. Grine

Terra Tek, Inc.
ATTN: A. Jones
ATTN: S. Green

TRW Defense & Space Sys. Group
ATTN: R1-2144, D. Jortner
ATTN: N. Lipner
ATTN: A. Feldman
ATTN: R1-2170, P. Dai
ATTN: R1-1104, P. Bhutta

TRW Defense & Space Sys. Group
San Bernardino Operations
ATTN: G. Hulcher
ATTN: 527/712, E. Wong
ATTN: F. Pieper

Universal Analytics, Inc.
ATTN: E. Field

The Eric H. Wang
Civil Engineering Rsch. Fac.
ATTN: N. Baum
ATTN: L. Bickle

Weidlinger Assoc. Consulting Engineers
ATTN: M. Baron

Weidlinger Assoc. Consulting Engineers
ATTN: J. Isenberg

Westinghouse Electric Corporation
Marine Division
ATTN: W. Volz